bioRxiv preprint doi: https://doi.org/10.1101/836023; this version posted November 8, 2019. The copyright holder for this preprint (which was not certified by peer review) is the author/funder, who has granted bioRxiv a license to display the preprint in perpetuity. It is made available under aCC-BY 4.0 International license.

The histone modification reader ZCWPW1 links histone methylation to repair of PRDM9-induced meiotic double stand breaks

Tao Huang[1,2,3,4,5,*], Shenli Yuan[7,*], Mengjing Li[1,2,3,4,5], Xiaochen Yu[1,2,3,4,5], Jianhong Zhang[7], Yingying Yin[1,2,3,4,5], Chao Liu[8], Lei Gao[7], Wei Li[8], Jiang Liu[7,#], Zi-Jiang Chen[1,2,3,4,5,6,#], Hongbin Liu[1,2,3,4,5,9,#]

[1]Center for Reproductive Medicine, Shandong Provincial Hospital Affiliated to Shandong University

[2]National Research Center for Assisted Reproductive Technology and Reproductive Genetics, China

[3]The Key laboratory of Reproductive Endocrinology (Shandong University), Ministry of Education

[4]Shandong Provincial Clinical Medicine Research Center for reproductive health

[5]Shandong Provincial Key Laboratory of Reproductive Medicine, No.157 Jingliu Road, Jinan, 250001, China

[6]Shanghai Key Laboratory for Assisted Reproduction and Reproductive Genetics, Shanghai ,China

[7]CAS Key Laboratory of Genome Sciences and Information, Beijing Institute of Genomics, Chinese Academy of Sciences, 100101 Beijing, China

[8]State Key Laboratory of Stem Cell and Reproductive Biology, Institute of Zoology, Chinese Academy of Sciences, Beijing 100101, China

[9]CUHK-SDU Joint Laboratory on Reproductive Genetics, School of Biomedical Sciences, the Chinese University of Hong Kong, Hong Kong, China

*These authors contributed equally to this work.

[#]Corresponding: liuj@big.ac.cn (JL); chenzijiang@hotmail.com (Z-JC); hongbin_sduivf@aliyun.com (HBL)

bioRxiv preprint doi: https://doi.org/10.1101/836023; this version posted November 8, 2019. The copyright holder for this preprint (which was not certified by peer review) is the author/funder, who has granted bioRxiv a license to display the preprint in perpetuity. It is made available under aCC-BY 4.0 International license.

ABSTRACT

It is known that the histone modification writer PRDM9 deposits H3K4me3 and H3K36me3 marks at future DSB sites very early in meiosis, the nature of any proteins which can read such marks is unknown. Here, we demonstrate *in vivo* that ZCWPW1 is a H3K4me3 reader and show that its binding at chromatin promotes completion of DSB repair and synapsis in mouse testes. Based on multiple ChIP-seq and immunofluorescence analyses with mutants—including an H3K4me3-reader-dead variant of ZCWPW1 mice line—we establish that ZCWPW1's occupancy on chromatin is strongly but not exclusively promoted by the histone-modification activity of the PRDM9. ZCWPW1 localizes to DMC1-labelled DSB hotspots in a largely PRDM9-dependent manner, where it facilitates completion of synapsis by mediating the DSB repair process. In sum, our study demonstrates the function of a reader protein that carries out work resulting from an epigenetics-based recombination hotspot selection system in mammals.

INTRODUCTION

Meiotic recombination promotes pairing and segregation of homologous chromosomes and disrupts linkage relationships, thus ensuring faithful genome transmission and increasing genetic diversity (Handel and Schimenti, 2010; Bolcun-Filas and Schimenti, 2012). At the molecular level, meiotic recombination is initiated by the induction of programmed DNA double-strand breaks (DSBs) that are repaired by homologous recombination, leading to gene conversion and crossing over (Hunter, 2015; Gray and Cohen, 2016; Zickler and Kleckner, 2015). DSB formation is a complex process, and DSB locations are known to be marked at the very earliest stages of meiosis by trimethylation of histone H3 on lysine 4 (H3K4me3) (de Massy, 2013; Baudat et al., 2013). In mammals, this is accomplished by the protein PRDM9, which is expressed in the leptotene and zygotene substages (Sun et al., 2015; Parvanov et al., 2017). PRDM9 is a DNA-binding zinc finger protein—it has a long and highly genetically variable zinc finger domain which determines its binding specificity (for defining recombination hotspots), while its SET domain possesses histone trimethyltransferase activity, and its KRAB domain is involved in protein-protein interactions (Grey et al., 2018; Paigen and Petkov, 2018). In yeast, the

bioRxiv preprint doi: https://doi.org/10.1101/836023; this version posted November 8, 2019. The copyright holder for this preprint (which was not certified by peer review) is the author/funder, who has granted bioRxiv a license to display the preprint in perpetuity. It is made available under aCC-BY 4.0 International license.

histone reader Spp1 links H3K4me3 sites at promoters with the DSB formation machinery, promoting DSB formation (Sommermeyer et al., 2013; Acquaviva et al., 2013). In mice, although multiple studies have shown that the H3K4me3 writer PRDM9 controls the locations for DSB formation (Myers et al., 2010; Parvanov et al., 2010; Baudat et al., 2010; Brick et al., 2012; Powers et al., 2016; Diagouraga et al., 2018; Grey et al., 2017), much less is known about the subsequent activities of any proteins which may read these epigenetic marks and thusly help advance the meiotic recombination process (Paigen and Petkov, 2018).

DSBs formation at sites defined by PRDM9 is catalyzed by an evolutionarily conserved topoisomerase-like enzyme complex consisting of the SPO11 enzyme and its binding partner TOPOVIBL (Bergerat et al., 1997; Keeney et al., 1997; Robert et al., 2016; Vrielynck et al., 2016; Panizza et al., 2011). After SPO11-mediated cleavage, there are single-strand overhang sequences which become coated with a number of proteins including DMC1 and RAD51 (Pittman et al., 1998; Tarsounas et al., 1999; Dai et al., 2017). The DSBs enable homology searching and alignment to occur, which in turn promote homology synapsis and DSB repair (Inagaki et al., 2010). The number of DSBs and the timing of their formation are known to be controlled by intersecting negative feedback circuits. A basic feature of meiosis is that DSB-mediated interactions and repair processes occur differentially between homologous nonsister chromatids, rather than between sisters, as occurs in mitotic DSB repair (Keeney et al., 2014; Lange et al., 2011; Garcia et al., 2015). Some DSBs are repaired in a way that generates crossovers (COs), wherein DNA is exchanged between homologous chromosomes (Baudat and de Massy, 2007). The ZMM proteins (*e.g.*, TEX11, MSH4/MSH5, and RNF212) are a group of functionally related proteins known for their roles in promoting the formation of COs (Kneitz et al., 2000; Edelmann et al., 1999; Yang et al., 2008; Lynn et al., 2007; Reynolds et al., 2013).

We previously reported that the zinc finger CW-type and PWWP domain containing 1 (ZCWPW1) protein is required for meiosis prophase I in mice, and noted that *Zcwpw1* deficiency disrupted spermatogenesis in male mice but did not disrupt oogenesis in females to the same extent (Li et al., 2019a). ZCWPW1 is a member of the CW-domain–containing protein family (Perry and Zhao, 2003; Liu et al., 2016). Its zinc finger CW (zf-CW) domain has three conserved tryptophan and four conserved

bioRxiv preprint doi: https://doi.org/10.1101/836023; this version posted November 8, 2019. The copyright holder for this preprint (which was not certified by peer review) is the author/funder, who has granted bioRxiv a license to display the preprint in perpetuity. It is made available under aCC-BY 4.0 International license.

cysteine residues, and structural analysis has indicated that human ZCWPW1's zf-CW domain is a histone modification reader (He et al., 2010), while chromatin pulldown analysis has confirmed that ZCWPW1's zf-CW domain recognizes H3K4me3 marks (Hoppmann et al., 2011). A crystal structure of the human zf-CW domain of ZCWPW1 in complex with a peptide bearing an H3K4me3 mark revealed that 4 amino acids largely mediate the H3K4me3 mark binding activity of ZCWPW1's zf-CW domain: W256, E301, T302, and W303 (He et al., 2010).

Here, we found in an immunofluorescence analysis of chromosome spreads from wild type, *Zcwpw1*$^{-/-}$, and mice expressing an H3K4me3-reader-dead mutant variant of the ZCWPW1 protein, that ZCWPW1 facilitates meiotic progression in mouse testes. A series of ChIP-seq analyses using antibodies against ZCWPW1, H3K4me3, and H3K36me3, assessing multiple knockout and knock-in mouse lines, establish that ZCWPW1 is an H3K4me3 and H3K36me3 reader which preferentially but not exclusively binds at genomic loci bearing PRDM9-deposited histone modifications. ZCWPW1 localizes to DMC1-labelled DSBs, where it can read H3K4me3 and H3K36me3 marks, and we confirm *in vivo* that ZCWPW1's H3K4me3 reader function contributes to meiotic recombination by greatly facilitating the DSB repair process. Thus, beyond demonstrating that a histone modification reader protein functions in an epigenetics-based recombination hotspot selection system, this study advances our understanding of the sequence of recruitment events that are required for crossover formation during meiosis.

RESULTS

ZCWPW1 is an H3K4me3 reader and its binding at chromosomal axes promotes completion of synapsis

We previously developed *Zcwpw1* knockout (KO) mice in the C57BL/6 genetic background in an earlier study (Li et al., 2019a), and in light of the known capacity of ZCWPW1 to recognize epigenetic methylation modification marks, we designed a knock-in strategy to generate a candidate H3K4me3 reader-dead mutant variant of ZCWPW1 (Fig. S1B). Specifically, this knock-in mutant variant of ZCWPW1 had three mutations: W247I /E292R /W294P. These mutations in murine ZCWPW1 are positionally equivalent to the previously reported W256I, E301R, and W303P mutations in the human

bioRxiv preprint doi: https://doi.org/10.1101/836023; this version posted November 8, 2019. The copyright holder for this preprint (which was not certified by peer review) is the author/funder, who has granted bioRxiv a license to display the preprint in perpetuity. It is made available under aCC-BY 4.0 International license.

ZCWPW1 protein, all of which are in its zf-CW domain, and all of which are known to be essential for the H3K4me3 reader function of human ZCWPW1 (He et al., 2010).

After checking that the ZCWPW1$^{W247I/E292R/W294P}$ variant protein was expressed at levels similar to wild type (WT) ZCWPW1 (Fig. S1C), we prepared testis sections from 8-week-old WT, *Zcwpw1*$^{-/-}$, and this new *Zcwpw1*$^{KI/KI}$ mice line. Hematoxylin staining revealed that spermatogenesis was disrupted in the *Zcwpw1*$^{-/-}$ and *Zcwpw1*$^{KI/KI}$ mice: the seminiferous tubules of WT mice appeared normal, while the *Zcwpw1*$^{-/-}$ and *Zcwpw1*$^{KI/KI}$ mice lacked post-meiotic cell types, contained apoptotic cells, or were nearly empty. Further, the WT epididymides were full of sperm, but there were no obvious sperm detected in either the *Zcwpw1*$^{-/-}$ or the *Zcwpw1*$^{KI/KI}$ samples, suggesting meiotic arrest (Fig. 1D).

These *in vivo* results, viewed alongside the previous reports about the function of ZCWPW1 in meiotic process and reports demonstrating that these specific mutations on ZCWPW1's zf-CW domain affect the protein's ability to read histone modifications including H3K4me3, together support that the ZCWPW1$^{W247I/E292R/W294P}$ variant is an H3K4me3-reader-dead variant of ZCWPW1. Further, these results establish that mice expressing an H3K4me3-reader-dead variant of ZCWPW1 have disrupted spermatogenesis.

We also analyzed chromosome spreads of spermatocytes from testes of PD60 mice via immunostaining for the synaptonemal complex (SC) markers SYCP1 and SYCP3 (Fig. 1E). The leptotene and zygotene meiotic chromosomes appeared normal for all of the genotypes. However, while synapsis occurred normally in the WT samples, extremely few instances of completed chromosomal synapsis were observed in the *Zcwpw1*$^{-/-}$ or *Zcwpw1*$^{KI/KI}$ mice, with spermatogenesis arresting in a pachytene-like stage. Thus, spermatocytes lacking the H3K4me3-reader activity of the ZCWPW1 protein have severely disrupted synapsis.

Having established that ZCWPW1 facilitates completion of synapsis during meiosis prophase I in male mice, and observed that a reader-dead ZCWPW1 variant causes the same meiotic arrest phenotypes as *Zcwpw1* genetic knockout, we next conducted chromatin immunoprecipitation sequencing (ChIP-seq) analysis using antibodies against the ZCWPW1 protein and against H3K4me3 marks. The ZCWPW1 ChIP-seq data for C57BL/6 mice revealed a total of 14,688 ZCWPW1 binding peaks, with 499 peaks localized within 2000 bp of a transcription start sites (TSS), 2,416 peaks localized

bioRxiv preprint doi: https://doi.org/10.1101/836023; this version posted November 8, 2019. The copyright holder for this preprint (which was not certified by peer review) is the author/funder, who has granted bioRxiv a license to display the preprint in perpetuity. It is made available under aCC-BY 4.0 International license.

in exons of protein-coding genes, 6,142 peaks localized in introns, as well as 5,873 peaks localized within intergenic regions (Fig. S2A).

A previously study found that 94% of DMC1-labeled hotspots overlap with H3K4me3 in testis, which can be considered a global feature of DSB sites in multicellular organisms (Smagulova et al., 2011). We found that the majority of ZCWPW1 peaks overlapped with H3K4me3 peaks in WT mice testes (Fig. 1A-B), supporting previous suppositions that these specifically overlapping H3K4me3 peaks may serve as ZCWPW1 recognizing histone modification marks.

Consistent with our ChIP-seq data, we conducted immunofluorescence analysis of chromosome spreads from spermatocytes of PD60 mice with the same two antibodies and found that H3K4me3 co-localized with ZCWPW1 in the leptotene and zygotene stages (Fig. S3A). We also conducted an additional ChIP-seq analysis of testes samples from PD14 WT, *Zcwpw1*$^{-/-}$, and *Zcwpw1*$^{KI/KI}$ mice. Obviously, this analysis indicated that no ZCWPW1 peaks were detected in the *Zcwpw1*$^{-/-}$ or *Zcwpw1*$^{KI/KI}$ mice (Fig. 1A/C). And this result suggests that the H3K4me3-reader function of this protein is essential for its capacity to bind on chromatin to function in meiosis prophase I in male mice.

ZCWPW1 binding is strongly promoted by the histone modification activity of PRDM9

To identify factor(s) responsible for ZCWPW1 recruitment to chromosomal axes *in vivo*, we searched for enriched motifs within the ZCWPW1 peak regions from our ChIP-seq data (Fig. S4A). This analysis identified a *de novo* motif, which is exactly the same as a known PRDM9 binding motif in C57BL/6J background mice (Fig. S4B) (Segurel, 2013; Billings et al., 2013; Walker et al., 2015), suggesting that ZCWPW1 deposition may act in a PRDM9-dependent manner. Pursuing this, we analyzed our ChIP-seq data with an anti-ZCWPW1 antibody alongside previously published ChIP-seq data for an anti-PRDM9 antibody (Grey et al., 2017). At the genome-wide level, 13% of the ZCWPW1 peaks overlapped with PRDM9 peaks. Conversely 1,934 of the 2,601 PRDM9 peaks (74%) from the previous study overlapped with ZCWPW1 peaks (Fig. 2A-B, Fig. S4C). Our further analysis of intensity of H3k4me3 peaks showed that among the Prdm9 dispositioned regions, compared with the regions non-overlapped with Zcwpw1, the intensity of H3k4me3 peaks overlapped Zcwpw1 were significantly weak (Fig. S2B). Allowing for differences in the binding performance of separate antibodies in separate ChIP-

bioRxiv preprint doi: https://doi.org/10.1101/836023; this version posted November 8, 2019. The copyright holder for this preprint (which was not certified by peer review) is the author/funder, who has granted bioRxiv a license to display the preprint in perpetuity. It is made available under aCC-BY 4.0 International license.

seq analyses, the fact that some but certainly not all of the ZCWPW1 peaks overlap with PRDM9 peaks suggest that it is the H3K4me3 and perhaps H3K36me3 epigenetic marks deposited by PRDM9, rather than the PRDM9 protein *per se*, which can explain the observed overlap of the ZCWPW1 and PRDM9 binding peaks.

Extending the insight about the overlap between ZCWPW1 and H3K4me3 peaks in our ChIP-seq data, and in light of the well-known overlap of PRDM9 peaks with H3K4me3 and H3K36me3 peaks (Grey et al., 2017), we found that the H3K36me3 peaks shared strong overlap with ZCWPW1 peaks (Fig. S2C-E). Consistent with the ChIP-seq data, we conducted immunofluorescence analysis of chromosome spreads from spermatocytes of PD60 mice with H3K36me3 and ZCWPW1 antibodies and found that H3k36me3 co-localized with ZCWPW1 in the leptotene and zygotene stages (Fig. S3B). We next conducted ChIP-seq analysis of testes from PD14 wild type and *Prdm9*$^{-/-}$ knockout mutant mice (Fig. 2D-E, Fig. S4D). Intriguingly, there were very few ZCWPW1 peaks for the *Prdm9*$^{-/-}$ mutant testes samples (only 759 peaks, vs. 14,668 ZCWPW1 peaks observed in the ChIP-seq analysis of the WT C57BL/6 mice), suggesting that ZCWPW1 binding is strongly promoted by the specific activity of PRDM9.

Analysis of the overlap of ZCWPW1, H3k4me3, and PRDM9 peaks in WT and *Prdm9*$^{-/-}$ testes showed that loss of PRDM9 function causes a sharp decrease in the extent of overlap between PRDM9 and ZCWPW1 peaks (Fig. 2D-E, Fig. S4D). We also examined whether *Prdm9*$^{-/-}$ mice had H3k4me3 peaks and H3K36me3 at the PRDM9 binding regions which we had detected in wild type mice: the number of such H3k4me3 peaks and H3K36me3 decreased sharply upon loss of PRDM9 function (Fig. 2D-E, Fig. S4D and S2E). However, in our ChIP-seq data, we showed that the H3K4me3 peaks overlap with PRDM9 but without ZCWPW1 have no obviously difference in wild type and *Prdm9*$^{-/-}$ testes. We speculated that other than PRDM9 acts as an indispensable methyltransferase in meiosis; it may also act as a reader in recognizing H3k4me3 modification.

ZCWPW1 localizes to DMC1-labelled DSB hotspots and does so in a PRDM9-dependent manner

A previous study reported a single-stranded DNA sequencing (SSDS) analysis using an antibody against DMC1 in C57BL/6 mice testes (Khil et al., 2012). We compared the distribution of the DMC1 peaks in

bioRxiv preprint doi: https://doi.org/10.1101/836023; this version posted November 8, 2019. The copyright holder for this preprint (which was not certified by peer review) is the author/funder, who has granted bioRxiv a license to display the preprint in perpetuity. It is made available under aCC-BY 4.0 International license.

that publically available data set with the ZCWPW1 peaks which we identified in our ChIP-seq analyses (Fig. S5A-C). For the WT mice, 11,124 of the 14,688 total ZCWPW1 peaks overlapped with DMC1-defined DSB hotspots. Our data for *Prdm9*$^{-/-}$ mice indicated an apparent lack of any overlap between DSB hotspots, ZCWPW1 peaks, and H3k4me3 signals (Fig. 3A-C). These data reinforce the idea that occupancy of ZCWPW1 at DSB hotspots is largely dependent on PRDM9-mediated histone modifications.

However, it bears mention that we also detected 3,609 ZCWPW1 peaks which did not obviously overlap DSB hotspots, and we found that only 759 such ZCWPW1 peaks were detected in the *Prdm9*$^{-/-}$mice (Fig. 3B-C). We analyzed these 759 binding sites in detail, and it was interesting to note that 626 of these peaks occurred within 5,000 bp of a TSS, a substantially larger proportion than for the average position among all hotspot ZCWPW1 peaks (Fig. S5D-G). Moreover, a GO analysis of each of these non-DSB-overlap protein-coding genes indicated enrichment for functional annotations related to embryonic development and spermatogenesis. Thus, although it is clear that the majority of the ZCWPW1 peaks result from PRDM9's activity, it is possible that ZCWPW1 may have an additional transcription regulation function that is not obviously related to the PRDM9-mediated hotspot selection system.

ZCWPW1 functions in meiotic recombination by facilitating DSB repair

Having established that ZCWPW1 is a reader of H3k4me3 marks which occur at chromosome sites preferentially accessed by the known meiosis-DSB-directing histone modification writer PRDM9, we speculated about the possible recombination-related function(s) of ZCWPW1. We performed immunofluorescence staining of chromosome spreads to evaluate recruitment of DMC1 and RAD51 to single-strand overhang sequences (hotspots) in wild type and *Zcwpw1*$^{KI/KI}$ mice (Fig. S6A-B). There were no differences in the numbers of DMC1 and RAD51 foci in the zygotene stage of the two genotypes. However, analysis of WT pachytene and *Zcwpw1*$^{KI/KI}$ pachytene-like spermatocytes revealed an obvious discrepancy. Decreased numbers of DMC1, RAD51 foci occurred in the pachytene wild type samples, indicating successful repair of DSBs, but *Zcwpw1*$^{KI/KI}$ pachytene-like samples retained a large number of DMC1, RAD51 foci. Indeed, there were actually many more DMC1 and RAD51 foci

bioRxiv preprint doi: https://doi.org/10.1101/836023; this version posted November 8, 2019. The copyright holder for this preprint (which was not certified by peer review) is the author/funder, who has granted bioRxiv a license to display the preprint in perpetuity. It is made available under aCC-BY 4.0 International license.

in *Zcwpw1*$^{KI/KI}$ pachytene-like spermatocytes than in WT pachytene spermatocytes, suggesting the ongoing accumulation of DSBs in the absence of a functional ZCWPW1 protein. These results suggest that ZCWPW1 facilitates meiotic DSB repair downstream of strand invasion.

Seeking to further assess the functional contribution(s) of ZCWPW1 in meiotic recombination, we analyzed chromosome spreads of spermatocytes from testes of PD60 WT, *Zcwpw1*$^{-/-}$ and *Zcwpw1*$^{KI/KI}$ mice with immunostaining against the SC marker SYCP3, the recombination factors MSH4 and RNF212, and the Holliday junction dissolution marker MLH1 (Fig. 4A-B, Fig. S6C). Staining against MSH4 and RNF212 revealed that the recombination machinery can apparently assemble normally in zygotene WT cells and in zygotene *Zcwpw1*$^{-/-}$ and *Zcwpw1*$^{KI/KI}$ cells. However, these MSH4 and RNF212 signals decreased as expected in WT pachytene cells, but persisted on the pachytene-like *Zcwpw1*$^{-/-}$ and *Zcwpw1*$^{KI/KI}$ chromosomes(Fig. 4A-B). Additionally, the MLH1 staining patterns indicated that Holliday junction dissolution proceeded normally in mid- to late-pachytene WT cells but indicated that the recombination processes remained ongoing in the pachytene-like cells lacking functional ZCWPW1, failing to progress to the pachytene stage: no crossover occurred, so no MLH1 foci could be observed (Fig. S6C). These results suggest that DSB repair is defective downstream of the formation of recombination intermediates in the *Zcwpw1*$^{-/-}$ and *Zcwpw1*$^{KI/KI}$ mice.

To determine the specific process that can mechanistically account for the observed failure to complete meiotic recombination, we analyzed chromosome spreads of spermatocytes from testes of PD60 WT, *Zcwpw1*$^{-/-}$, and *Zcwpw1*$^{KI/KI}$ mice. Staining of leptotene and zygotene cells against the DSB site marker γH2AX and the SC marker SYCP3 showed that DSBs can form normally in all of the genotypes (Fig. 5A). However, there were obvious differences between pachytene WT spermatocytes and pachytene-like *Zcwpw1*$^{-/-}$ and *Zcwpw1*$^{KI/KI}$ spermatocytes: WT pachytene spermatocyte exhibited no obvious signal for DSB sites on auto chromosomes except the sex chromosome, while both *Zcwpw1*$^{-/-}$ and *Zcwpw1*$^{KI/KI}$ pachytene-like chromosomes retained obvious γH2AX signals. Moreover, XY bodies had formed in the WT pachytene spermatocytes but were not observed in the pachytene-like *Zcwpw1*$^{-/-}$ and *Zcwpw1*$^{KI/KI}$ spermatocytes. We next stained against the DSB-repair machinery component p-ATM and found—consistent with the persistent DSBs in pachytene-like spermatocyte lacking functional ZCWPW1—that DSB repair was apparently ongoing in the pachytene-like *Zcwpw1*$^{-/-}$ or *Zcwpw1*$^{KI/KI}$

bioRxiv preprint doi: https://doi.org/10.1101/836023; this version posted November 8, 2019. The copyright holder for this preprint (which was not certified by peer review) is the author/funder, who has granted bioRxiv a license to display the preprint in perpetuity. It is made available under aCC-BY 4.0 International license.

cells(Fig. 5B). These data indicate that ZCWPW1 is dispensable for the induction of DSBs; rather, ZCWPW1 is required for proper interhomologue interactions including synapsis and the repair of DSBs that occur in later steps of homologous recombination.

DISCUSSION

Our data support a working model wherein PRDM9 binds to specific DNA motifs in the genome and writes histone modifications (H3K4me3 and H3K36me3) via the methyltransferase activity of its PR/SET domain (Powers et al., 2016; Diagouraga et al., 2018). This leads to the recruitment of proteins required for the formation of DSBs in the vicinity of its binding site (e.g., SPO11, etc.) (Panizza et al., 2011; Stanzione et al., 2016; Tesse et al., 2017; Kumar et al., 2018). After these PRDM9-catalyzed epigenetic modifications are deposited, ZCWPW1 can specifically read these H3K4me3 and H3K36me3 marks in the vicinity of DSB sites, where it functions to somehow promote DSB repair. This DSB-repair-promoting function obviously greatly increases the overall completion rates of synapsis, crossover formation, and ultimately meiotic progression.

The identification of recombination hotspots was first made in genetically-tractable experimental organisms such as bacteriophages and fungi, but it is now apparent that hotspots are ubiquitous and active in apparently all organisms (Wahls, 1998). Higher-order chromosome architecture, which can be described using terminology of the “tethered-loop/axis complex” model, contributes to DSB hotspot localization (Blat et al., 2002). Different strategies and mechanisms for the spatial regulation of DSB formation have evolved in different species, although commonalities exist (de Massy, 2013; Baudat et al., 2013). By considering the evolution of hotspot selection systems, we have become interested in whether other meiotic factors may have evolved in vertebrates to link PRDM9 to the machinery of meiotic recombination and/or the synaptonemal complex, which permit direct interactions with the histone marks deposited by PRDM9.

In *S. cerevisiae*, Spp1—whose PHD finger domain is known to read H3K4me3 marks— promotes meiotic DSB formation by interacting with the axis-bound Spo11 accessory protein Mer2 (Sommermeyer et al., 2013; Acquaviva et al., 2013). In mammals, our study supports that another, as-yet unknown protein(s) may function in a similar role during DSB formation. It is noteworthy that there

bioRxiv preprint doi: https://doi.org/10.1101/836023; this version posted November 8, 2019. The copyright holder for this preprint (which was not certified by peer review) is the author/funder, who has granted bioRxiv a license to display the preprint in perpetuity. It is made available under aCC-BY 4.0 International license.

is structural similarity between the zf-CW domain and the PHD finger of Spp1 that helps recognize histone H3 tails (Adams-Cioaba and Min, 2009). Moreover, structural analysis has indicated that human ZCWPW1's zf-CW domain is a histone modification reader (He et al., 2010), and chromatin pulldown analysis has confirmed that ZCWPW1's zf-CW domain recognizes H3K4me3 marks (Hoppmann et al., 2011). In the present study, we showed that ZCWPW1 can specifically read H3K4me3 and H3K36me3 marks in the vicinity of DSB sites. However, somewhat surprisingly, our subsequent experiments indicated that deficiency of ZCWPW1 does not affect the recruitment of recombination-related factors like DMC1, MSH4, and RNF212, thereby implying there may be other unknown protein(s) which function to link PRDM9 to the DSB machinery.

ZCWPW1 possesses a Zinc Finger CW-Type domain and a PWWP domain. The zf-CW domain has previously been shown to bind to the H3K4me3 peptides (He et al., 2010). The PWWP domain, another type of 'reader' module, has been demonstrated to recognize H3K36me3 in the peptide and nucleosome contexts (Eidahl et al., 2013; Rondelet et al., 2016; Vezzoli et al., 2010). Consistent with a recently deposited pre-print at bioRxiv which showed, *in vitro*, that ZCWPW1 can bind to histone H3 peptides with double H3K4me3 and H3K36me3 marks with high affinity at a 1:1 ratio (Mahgoub et al., 2019), we also found that ZCWPW1 is localized to H3K4me3 and H3K36me3 enrichment regions in our ChIP-seq analysis. Notably, most of ZCWPW1 peaks overlapping H3K4me3 peaks disappeared in *Prdm9*-null mice. One functional purport of our study is that it is PRDM9's histone modification activity, rather than the chromatin residence of the PRDM9 protein *per se*, which can account for the functional interactions of the apparently co-involved ZCWPW1 and PRDM9 proteins.

Our H3K4me3-reader-dead mutant mice results showed *in vivo* that, upon disruption of the binding capacity of the ZCWPW1's Zinc Finger CW-Type domain for H3K4me3 marks, the ZCWPW1 protein completely lost its ability to bind chromosome axes, and spermatocytes in mice expressing this knock-in H3K4me3-reader-dead variant ZCWPW1 exhibited a near-complete failure of meiosis prophase I. It remains unclear whether ZCWPW1's PWWP domain (which likely functions in reading H3K36me3 mark) and/or other regions of the ZCWPW1 protein confer similarly impactful functions. Indeed, we anticipate that our future work will pursue the selective disruption of the function of particular ZCWPW1 domains in our attempts to elucidate this protein's function(s) in male meiosis I. A detailed

bioRxiv preprint doi: https://doi.org/10.1101/836023; this version posted November 8, 2019. The copyright holder for this preprint (which was not certified by peer review) is the author/funder, who has granted bioRxiv a license to display the preprint in perpetuity. It is made available under aCC-BY 4.0 International license.

prediction analysis of potential binding sites for ZCWPW1 based on our ChIP-data indicated that there are 499 ZCWPW1 binding sites located within 2000bp of the TSS regions of protein-encoding genes, and a GO analysis suggested that many of these genes have functions relating to meiosis. We speculate that ZCWPW1 may exert a function as a transcription factor which controls the timely transcription of meiosis-related genes.

While we clearly show that ZCWPW1 greatly facilitates PRDM9-dependent DSB repair, we do not yet have strong evidence suggesting the precise nature of its functional role. One possibility is that ZCWPW1, upon binding to PRDM9-dependent histone modification hotspots, may serve as a DSB mark, which can perhaps subsequently recruit other factors involved in DSB repair. Recent studies have reported that PRDM9 binds on both the cut and uncut template chromosomes to promote meiotic recombination (Hinch et al., 2019; Li et al., 2019b). It is also possible that ZCWPW1 may directly interact with SC machinery through its SCP1-like domain to tether PRDM9-bound loops to the SC to promote homologous DSB repair.

In summary, our study identifies ZCWPW1 as an H3K4me3 and H3K36me3 reader that promotes repair of DNA double-strand breaks during meiotic recombination, excluding previous suppositions that perhaps this protein directs the location or the formation of DSBs (Mahgoub et al., 2019; Wells et al., 2019). In future studies, we plan to focus on additional proteins (*e.g.*, ZCWPW2, MORC3/4 etc.) which have similar functional domains with ZCWPW1 (Liu et al., 2016), with the aim of identifying any unknown biomolecules which act to link PRDM9 to the DSB machinery specifically or to meiotic recombination more generally.

MATERIALS AND METHODS

Mice

The *Zcwpw1* gene (NCBI Reference Sequence: NM_001005426.2) is located on mouse chromosome 5 and comprises 17 exons, with its ATG start codon in exon 2 and a TAG stop codon in exon 17. The *Zcwpw1* knockout mice were generated in our previous study (Li et al., 2019a). The *Zcwpw1* knock-in H3K4me3-reader-dead mutant mice were generated by mutating 3 sites. The W247I (TGG to ATT) point mutation was introduced into exon 8 in 5' the homology arm, and the E292R (GAG to CGG) and

bioRxiv preprint doi: https://doi.org/10.1101/836023; this version posted November 8, 2019. The copyright holder for this preprint (which was not certified by peer review) is the author/funder, who has granted bioRxiv a license to display the preprint in perpetuity. It is made available under aCC-BY 4.0 International license.

W294P (TGG to CCG) point mutations were introduced into exon 9 in the 3' homology arm. The W247I (TGG to ATT), E292R (GAG to CGG), and W294P (TGG to CCG) mutations created in the mouse *Zcwpw1* gene are positionally equivalent to the W256I, E301R, and W303P mutations previously reported in the human *ZCWPW1* gene. To engineer the targeting vector, homology arms were generated by PCR using BAC clones RP24-387B18 and RP24-344E7 from the C57BL/6 library as templates. In the targeting vector, the Neo cassette was flanked by SDA (self-deletion anchor) sites. DTA was used for negative selection. C57BL/6 ES cells were used for gene targeting. Genotyping was performed by PCR amplification of genomic DNA extracted from mouse tails. PCR primers for the *Zcwpw1* Neo deletion were Forward: 5'-CACTGAGTTAATCCCACCTACGTC-3' and Reverse: 5'CTCTCCCAAACCATCTCAAACATT-3', with targeted point mutants yielding a 318 bp fragment and wild type mice yielding a 174 bp fragment.

The mouse *Prdm9* gene (GenBank accession number: NM_144809.3) is located on mouse chromosome 17. Ten exons have been identified, with the ATG start codon in exon 1 and TAA stop codon in exon 10. The *Prdm9* knockout mice in a C57BL/6 genetic background were generated by deleting the genomic DNA fragment covering exon 1 to exon 9 using the CRISPR/Cas9-mediated genome editing system (performed commercially by Cyagen Biosciences). The founders were genotyped by PCR followed by DNA sequencing analysis. Genotyping was performed by PCR amplification of genomic DNA extracted from mouse tails. PCR primers for the *Prdm9* mutant allele were Forward: 5'-GCTTAGGTAGCAGAATTGAAGGGAAAGTC-3' and Reverse: 5'-GTTTGTGTCTTTCTAACTCAAACTTCTGCA-3', yielding a 580 bp fragment. PCR primers for the *Prdm9* wild type allele were Forward: 5'- GCTTAGGTAGCAGAATTGAAGGGAAAGTC-3' and Reverse: 5'- TCGTGGCGTAATAATAGAGTGCCTTG-3', yielding a 401 bp fragment.

All mice were housed under controlled environmental conditions with free access to water and food, and illumination was on between 6 am and 6 pm. All experimental protocols were approved by the Animal Ethics Committee of the School of Medicine of Shandong University.

Tissue collection and histological analysis

bioRxiv preprint doi: https://doi.org/10.1101/836023; this version posted November 8, 2019. The copyright holder for this preprint (which was not certified by peer review) is the author/funder, who has granted bioRxiv a license to display the preprint in perpetuity. It is made available under aCC-BY 4.0 International license.

Testes from least three mice for each genotype were dissected immediately after euthanasia, fixed in 4% (mass/vol) paraformaldehyde (Solarbio) for up to 24 h, stored in 70% ethanol, and embedded in paraffin after dehydration, and 5 μm sections were prepared and mounted on glass slides. After deparaffinization, slides were stained with hematoxylin for histological analysis using an epifluorescence microscope (BX52, Olympus); images were processed using Photoshop (Adobe).

Chromosome spread immunofluorescence analysis

Spermatocyte spreads were prepared as previously described (Peters et al., 1997). Primary antibodies used for immunofluorescence were as follows: rabbit anti-ZCWPW1 (1:1,000 dilution; homemade(Li et al., 2019a)), mouse anti-SCP3 (1:500 dilution; Abcam #ab97672), rabbit anti-SCP1 (1:2,000 dilution; Abcam # ab15090), rabbit anti-RAD51 (1:200 dilution; Thermo Fisher Scientific #PA5-27195), rabbit anti-DMC1 (1:100 dilution; Santa Cruz Biotechnology #sc-22768), mouse anti-γH2AX (1:300 dilution; Millipore #05-636), mouse anti-pATM (1:500 dilution; Sigma-Aldrich # 05-740), rabbit anti-MSH4 (1:500 dilution; Abcam #ab58666), RNF212 (1:500 dilution; a gift from Mengcheng Luo, Wuhan University), mouse anti-MLH1 (1:50 dilution; BD Biosciences #550838), rabbit anti-H3K4me3 (1:500 dilution; Abcam #ab8580), and rabbit anti-H3K36me3 (1:500 dilution; Abcam #ab9050). Primary antibodies were detected with Alexa Fluor 488-, 594-, or 647-conjugated secondary antibodies (1:500 dilution, Thermo Fisher Scientific #A-11070, Abcam #ab150084, #ab150067, #ab150113, #ab150120, #ab150119, #ab150165, #ab150168, and #ab150167) for 1 h at room temperature. The slides were washed with PBS for several times and mounted using VECTASHIELD medium with DAPI (Vector Laboratories, # H-1200). Immunolabeled chromosome spreads were imaged by confocal microscopy using a Leica TCS SP5 resonant-scanning confocal microscope. Projection images were then prepared using ImageJ Software (NIH, Ver. 1.6.0-65) or Bitplane Imaris (version8.1) software.

Immunoblotting

To prepare protein extracts, tissues were collected from male C57BL/6 mice and lysed in TAP lysis buffer (50 mM HEPES-KOH, pH 7.5, 100 mM KCl, 2 mM EDTA, 10% glycerol, 0.1% NP-40, 10 mM NaF, 0.25 mM Na3VO4, 50 mM β-glycerolphosphate) plus protease inhibitors (Roche, 04693132001)

bioRxiv preprint doi: https://doi.org/10.1101/836023; this version posted November 8, 2019. The copyright holder for this preprint (which was not certified by peer review) is the author/funder, who has granted bioRxiv a license to display the preprint in perpetuity. It is made available under aCC-BY 4.0 International license.

for 30 min on ice, followed by centrifugation at 4°C at 13,000 × g for 15 min. The supernatant were used for Western blotting. Equal amounts of protein were electrophoresed on 10% Bis-Tris Protein Gels (Invitrogen, NP0315), and the bands were transferred to polyvinylidene fluoride membranes (Millipore). The primary antibodies for immunoblotting included anti-tubulin (1:10,000 dilution; Proteintech Group, #11224-1-AP), and anti-ZCWPW1 (1:5,000 dilution; homemade). Immunoreactive bands were detected and analyzed with a Bio-Rad ChemiDoc MP Imaging System and Image Lab Software (Bio-Rad).

ChIP-seq experiments

The collected cells from testes were cross-linked in 100 μL of 1% formaldehyde in PBS at room temperature for 10 min. 25 μL 1.25M glycine solution was added, followed by mixing via gentle tapping and incubation at room temperature for 5 min. After that, the cell pellet was washed in PBS for three times. Dynabeads Protein A beads (Life Technologies, 10001D) of 25 μL were washed twice with 200 μL ice-cold 140 mM RIPA buffer (10 mM Tris-HCl pH 7.5, 140 mM NaCl, 1 mM EDTA, 0.5 mM EGTA, 0.1% SDS, 0.1% Na-deoxycholate, 1% Triton X-100, 1mM PMSF, 1x Cocktail proteinase inhibitor, 20 mM Na-butyrate), followed by resuspension in RIPA buffer to a final volume of 200 μL in a 1.5ml tube. 5 μl H3K4me3 antibody (Abcam, ab8580) or 7μl ZCWPW1 antibody (homemade, 5ug/μl) or 5μl H3K36me3 antibody(Abcam, ab9050) was added into the beads suspension, followed by incubation on a tube rotator for at least 2.5 hrs at 4°C. The antibody-coated beads were then washed twice in 140mM RIPA buffer, followed by resuspension with 200 μL 140mM RIPA buffer.

The cross-linked cells were incubated in 150 μL lysis buffer (50 mM Tris-HCl pH 8.0, 10 mM EDTA pH8.0, 0.5% SDS, 1mM PMSF, 1x proteinase inhibitor cocktail, 20 mM Na-butyrate) for 20 min on ice, then sonicated using a Diagenode Bioruptor sonication device for 23 cycles (30s ON and then 30s OFF). 150μl 300mM RIPA [No SDS] (10 mM Tris-HCl pH 7.5, 300 mM NaCl, 1 mM EDTA, 0.5 mM EGTA, 1% Triton X-100, 0.1% Na-deoxycholate, 1mM PMSF, 1x Cocktail proteinase inhibitor, 20 mM Na-butyrate) and 200μl 140mM RIPA [No SDS] were added to the samples. After centrifugation at 13,000 × g for 10 min at 4°C, 40 μL supernatant was taken out and used as sample input. The

bioRxiv preprint doi: https://doi.org/10.1101/836023; this version posted November 8, 2019. The copyright holder for this preprint (which was not certified by peer review) is the author/funder, who has granted bioRxiv a license to display the preprint in perpetuity. It is made available under aCC-BY 4.0 International license.

remaining supernatant was transferred to a 1 ml tube containing suspended antibody-coated Protein A beads, followed by incubation on a tube rotator overnight at 4°C.

For the H3K4me3 and H3K36me3 antibodies, the incubated Protein A beads were washed once with RIPA buffer containing 250 mM NaCl, three times with RIPA buffer containing 500 mM NaCl, and once with TE buffer (10 mM Tris-HCl pH 8.0, 1mM EDTA). For the ZCWPW1 antibody, the incubated Protein A beads were washed twice with RIPA buffer containing 250 mM NaCl, once with RIPA buffer containing 500mM NaCl, and once with TE buffer for one time. Next, the beads were transferred to a new 0.5ml tube, followed by incubation in 100 μL ChIP elution buffer (10mM Tris-HCl pH8.0, 5mM EDTA, 300mM NaCl, 0.5% SDS) containing 5 μL proteinase K (Qiagen, 20mg/ml stock) at 55°C for 2 h, 65°C for 4 h. The eluate was transferred to a 0.5 mL tube. The enriched DNA was purified by phenol–chloroform, followed by dissolution in 50 μL TE buffer.

An NEBNext Ultra II DNA Library Prep Kit for Illumina (NEB, E7645S) was used for library construction according to product instructions. DNA was first end repaired and A-tailed by adding 7 μL NEBNext Ultra II End Prep Reaction Buffer and 3 μL NEBNext Ultra II End Prep Enzyme Mix. Samples were incubated at 20°C for 30min, 65°C for 30min, and finally cooled to 4°C in a thermal cycler. Adaptor ligation was performed by adding 30 μL NEBNext Ultra II Ligation Master Mix, 1 μL NEBNext Ligation Enhancer, 0.8 μL 200mM ATP, and 2.5 μL 15 μM Illumina Multiplexing Adaptors. Samples were thoroughly mixed and incubated at 20°C for 40 min. Following adaptor ligation, 1.2 volume SPRIselect beads (Beckman Coulter, B23318) were used to purify DNA. PCR amplification was performed with NEBNext Ultra II Q5 Master Mix. The PCR cycle number was evaluated using a FlashGelTM System (Lonza, 57063). The volume of the PCR product was adjusted to 100 μL by adding 50 μl TE buffer. The 300-700 bp DNA fragments were selected with 0.5 volume plus 0.5 volume SPRIselect beads, then eluted in 20 μL water. The libraries were sequenced on a Hiseq X-ten instrument set for paired-end 150 bp sequencing (Illumina).

ChIP-seq Bioinformatics Analysis

The ChIP-seq raw reads were cropped to 100 bp, and the low quality reads were removed using Trimmomatic v0.32 (Bolger et al., 2014). Paired reads were mapped to the mouse genome (version

bioRxiv preprint doi: https://doi.org/10.1101/836023; this version posted November 8, 2019. The copyright holder for this preprint (which was not certified by peer review) is the author/funder, who has granted bioRxiv a license to display the preprint in perpetuity. It is made available under aCC-BY 4.0 International license.

mm10) by Bowtie2 v2.3.4.2 with parameters "-X 2000 -no-discordant –no-contain" (Langmead and Salzberg, 2012). Reads with low mapping quality (MAPQ < 10) and PCR duplicated reads were removed by Samtools and Picard (DePristo et al., 2011; Li et al., 2009). The H3K4me3 peaks were called by MACS2 v2.1.0 (Zhang et al., 2008) with parameters "-keep-dup all -SPMR -p 0.01 –nomodel, ZCWPW1 peaks with parameters --keep-dup all -SPMR -p 0.001 –nomodel, H3K36me3 peaks with parameters -B --SPMR --broad –nomodel. DMC1 and PRDM9 raw data and peaks were directly obtained from the paper above, and transformed to mm10 by the LiftOver application from UCSC. ZCWPW1 peaks were further selected based on intensity greater than a 3-fold enrichment over the input lambda. The normalized signals of H3K4me3, H3K36me3, ZCWPW1, PRDM9, and DMC1 were generated using macs2 bdgcmp, following the output produced by macs2 Callpeak with SPRM (reads per million for each covered position). The Fold Change over lamda worked as signal enrichment, and transformed into Bigwig by bedGraphToBigWig. ChIP-seq signal tracks were visualized by Integrative Genomics Viewer (IGV) (Robinson et al., 2011). Deeptools2 (Ramirez et al., 2016) and R (3.4.4) were used to generate the profile plot and heatmap. The script findMotifsGenome.pl function in HOMER software (Heinz et al., 2010) was used to examine enrichment for transcription factor binding motifs. GO analysis conducted using Metascape (Zhou et al., 2019). The gene-region association and ontology analysis in Mouse Phenotye Single KO were fulfilled by GREATER software (McLean et al., 2010). All analyses for inferential statistical significance (p value) were obtained through Mann-Whitney U Tests.

Author contributions

Tao Huang performed ChIP-seq, analyzed and interpreted the data, wrote and edited the manuscript; Shenli Yuan performed ChIP-seq and data analysis; Mengjing Li, Xiaochen Yu performed Western blot and IF experiments, helped write and edit the manuscript; Yingying Yin bred the mice and performed the Western blot; Jianhong Zhang and Lei Gao provided guidance of ChIP-seq; Chao Liu and Wei Li discussed the mouse model construction and the ChIP-seq strategy; Jiang Liu, Zi-Jiang Chen and Hongbin Liu supervised the study, wrote and edited the manuscript.

bioRxiv preprint doi: https://doi.org/10.1101/836023; this version posted November 8, 2019. The copyright holder for this preprint (which was not certified by peer review) is the author/funder, who has granted bioRxiv a license to display the preprint in perpetuity. It is made available under aCC-BY 4.0 International license.

Acknowledgments

We are grateful for the interesting discussion with K. Liu from the University of Hong Kong, China, in the very initial phase of the study. Funding: This work was supported by the National Key Research and Development Programs of China [2018YFC1003400] and the Major Program of National Natural Science Foundation of China [31890780].

Declaration of interests

The authors declare no competing interests.

References

1. Handel MA and Schimenti JC. Genetics of mammalian meiosis: regulation, dynamics and impact on fertility. *Nature reviews Genetics*. 2010; 11: 124-36. doi:10.1038/nrg2723.
2. Bolcun-Filas E and Schimenti JC. Genetics of meiosis and recombination in mice. *International review of cell and molecular biology*. 2012; 298: 179-227. doi:10.1016/B978-0-12-394309-5.00005-5.
3. Hunter N. Meiotic Recombination: The Essence of Heredity. *Cold Spring Harbor perspectives in biology*. 2015; 7. doi:10.1101/cshperspect.a016618.
4. Gray S and Cohen PE. Control of Meiotic Crossovers: From Double-Strand Break Formation to Designation. *Annual review of genetics*. 2016; 50: 175-210. doi:10.1146/annurev-genet-120215-035111.
5. Zickler D and Kleckner N. Recombination, Pairing, and Synapsis of Homologs during Meiosis. *Cold Spring Harbor perspectives in biology*. 2015; 7. doi:10.1101/cshperspect.a016626.
6. de Massy B. Initiation of meiotic recombination: how and where? Conservation and specificities among eukaryotes. *Annual review of genetics*. 2013; 47: 563-99. doi:10.1146/annurev-genet-110711-155423.
7. Baudat F, Imai Y and de Massy B. Meiotic recombination in mammals: localization and regulation. *Nature reviews Genetics*. 2013; 14: 794-806. doi:10.1038/nrg3573.
8. Sun F, Fujiwara Y, Reinholdt LG, et al. Nuclear localization of PRDM9 and its role in meiotic chromatin modifications and homologous synapsis. *Chromosoma*. 2015; 124: 397-415. doi:10.1007/s00412-015-0511-3.

bioRxiv preprint doi: https://doi.org/10.1101/836023; this version posted November 8, 2019. The copyright holder for this preprint (which was not certified by peer review) is the author/funder, who has granted bioRxiv a license to display the preprint in perpetuity. It is made available under aCC-BY 4.0 International license.

9. Parvanov ED, Tian H, Billings T, et al. PRDM9 interactions with other proteins provide a link between recombination hotspots and the chromosomal axis in meiosis. *Molecular biology of the cell*. 2017; 28: 488-99. doi:10.1091/mbc.E16-09-0686.

10. Grey C, Baudat F and de Massy B. PRDM9, a driver of the genetic map. *PLoS genetics*. 2018; 14: e1007479. doi:10.1371/journal.pgen.1007479.

11. Paigen K and Petkov PM. PRDM9 and Its Role in Genetic Recombination. *Trends in genetics : TIG*. 2018; 34: 291-300. doi:10.1016/j.tig.2017.12.017.

12. Sommermeyer V, Beneut C, Chaplais E, Serrentino ME and Borde V. Spp1, a member of the Set1 Complex, promotes meiotic DSB formation in promoters by tethering histone H3K4 methylation sites to chromosome axes. *Molecular cell*. 2013; 49: 43-54. doi:10.1016/j.molcel.2012.11.008.

13. Acquaviva L, Szekvolgyi L, Dichtl B, et al. The COMPASS subunit Spp1 links histone methylation to initiation of meiotic recombination. *Science*. 2013; 339: 215-8. doi:10.1126/science.1225739.

14. Myers S, Bowden R, Tumian A, et al. Drive against hotspot motifs in primates implicates the PRDM9 gene in meiotic recombination. *Science*. 2010; 327: 876-9. doi:10.1126/science.1182363.

15. Parvanov ED, Petkov PM and Paigen K. Prdm9 controls activation of mammalian recombination hotspots. *Science*. 2010; 327: 835. doi:10.1126/science.1181495.

16. Baudat F, Buard J, Grey C, et al. PRDM9 is a major determinant of meiotic recombination hotspots in humans and mice. *Science*. 2010; 327: 836-40. doi:10.1126/science.1183439.

17. Brick K, Smagulova F, Khil P, Camerini-Otero RD and Petukhova GV. Genetic recombination is directed away from functional genomic elements in mice. *Nature*. 2012; 485: 642-5. doi:10.1038/nature11089.

18. Powers NR, Parvanov ED, Baker CL, Walker M, Petkov PM and Paigen K. The Meiotic Recombination Activator PRDM9 Trimethylates Both H3K36 and H3K4 at Recombination Hotspots In Vivo. *PLoS genetics*. 2016; 12: e1006146. doi:10.1371/journal.pgen.1006146.

19. Diagouraga B, Clement JAJ, Duret L, Kadlec J, de Massy B and Baudat F. PRDM9 Methyltransferase Activity Is Essential for Meiotic DNA Double-Strand Break Formation at Its Binding Sites. *Molecular cell*. 2018; 69: 853-65 e6. doi:10.1016/j.molcel.2018.01.033.

20. Grey C, Clement JA, Buard J, et al. In vivo binding of PRDM9 reveals interactions with noncanonical genomic sites. *Genome research*. 2017; 27: 580-90. doi:10.1101/gr.217240.116.

21. Bergerat A, de Massy B, Gadelle D, Varoutas PC, Nicolas A and Forterre P. An atypical topoisomerase II from Archaea with implications for meiotic recombination. *Nature*. 1997; 386: 414-7. doi:10.1038/386414a0.

22. Keeney S, Giroux CN and Kleckner N. Meiosis-specific DNA double-strand breaks are catalyzed by Spo11, a member of a widely conserved protein family. *Cell*. 1997; 88: 375-84. doi:10.1016/s0092-8674(00)81876-0.

bioRxiv preprint doi: https://doi.org/10.1101/836023; this version posted November 8, 2019. The copyright holder for this preprint (which was not certified by peer review) is the author/funder, who has granted bioRxiv a license to display the preprint in perpetuity. It is made available under aCC-BY 4.0 International license.

23. Robert T, Nore A, Brun C, et al. The TopoVIB-Like protein family is required for meiotic DNA double-strand break formation. *Science*. 2016; 351: 943-9. doi:10.1126/science.aad5309.
24. Vrielynck N, Chambon A, Vezon D, et al. A DNA topoisomerase VI-like complex initiates meiotic recombination. *Science*. 2016; 351: 939-43. doi:10.1126/science.aad5196.
25. Panizza S, Mendoza MA, Berlinger M, et al. Spo11-accessory proteins link double-strand break sites to the chromosome axis in early meiotic recombination. *Cell*. 2011; 146: 372-83. doi:10.1016/j.cell.2011.07.003.
26. Pittman DL, Cobb J, Schimenti KJ, et al. Meiotic prophase arrest with failure of chromosome synapsis in mice deficient for Dmc1, a germline-specific RecA homolog. *Molecular cell*. 1998; 1: 697-705. doi:10.1016/s1097-2765(00)80069-6.
27. Tarsounas M, Morita T, Pearlman RE and Moens PB. RAD51 and DMC1 form mixed complexes associated with mouse meiotic chromosome cores and synaptonemal complexes. *The Journal of cell biology*. 1999; 147: 207-20. doi:10.1083/jcb.147.2.207.
28. Dai J, Voloshin O, Potapova S and Camerini-Otero RD. Meiotic Knockdown and Complementation Reveals Essential Role of RAD51 in Mouse Spermatogenesis. *Cell reports*. 2017; 18: 1383-94. doi:10.1016/j.celrep.2017.01.024.
29. Inagaki A, Schoenmakers S and Baarends WM. DNA double strand break repair, chromosome synapsis and transcriptional silencing in meiosis. *Epigenetics*. 2010; 5: 255-66. doi:10.4161/epi.5.4.11518.
30. Keeney S, Lange J and Mohibullah N. Self-organization of meiotic recombination initiation: general principles and molecular pathways. *Annual review of genetics*. 2014; 48: 187-214. doi:10.1146/annurev-genet-120213-092304.
31. Lange J, Pan J, Cole F, Thelen MP, Jasin M and Keeney S. ATM controls meiotic double-strand-break formation. *Nature*. 2011; 479: 237-40. doi:10.1038/nature10508.
32. Garcia V, Gray S, Allison RM, Cooper TJ and Neale MJ. Tel1(ATM)-mediated interference suppresses clustered meiotic double-strand-break formation. *Nature*. 2015; 520: 114-8. doi:10.1038/nature13993.
33. Baudat F and de Massy B. Regulating double-stranded DNA break repair towards crossover or non-crossover during mammalian meiosis. *Chromosome research : an international journal on the molecular, supramolecular and evolutionary aspects of chromosome biology*. 2007; 15: 565-77. doi:10.1007/s10577-007-1140-3.
34. Kneitz B, Cohen PE, Avdievich E, et al. MutS homolog 4 localization to meiotic chromosomes is required for chromosome pairing during meiosis in male and female mice. *Genes & development*. 2000; 14: 1085-97.
35. Edelmann W, Cohen PE, Kneitz B, et al. Mammalian MutS homologue 5 is required for chromosome pairing in meiosis. *Nature genetics*. 1999; 21: 123-7. doi:10.1038/5075.
36. Yang F, Gell K, van der Heijden GW, et al. Meiotic failure in male mice lacking an X-linked factor. *Genes & development*. 2008; 22: 682-91. doi:10.1101/gad.1613608.

bioRxiv preprint doi: https://doi.org/10.1101/836023; this version posted November 8, 2019. The copyright holder for this preprint (which was not certified by peer review) is the author/funder, who has granted bioRxiv a license to display the preprint in perpetuity. It is made available under aCC-BY 4.0 International license.

37. Lynn A, Soucek R and Borner GV. ZMM proteins during meiosis: crossover artists at work. *Chromosome research : an international journal on the molecular, supramolecular and evolutionary aspects of chromosome biology*. 2007; 15: 591-605. doi:10.1007/s10577-007-1150-1.

38. Reynolds A, Qiao H, Yang Y, et al. RNF212 is a dosage-sensitive regulator of crossing-over during mammalian meiosis. *Nature genetics*. 2013; 45: 269-78. doi:10.1038/ng.2541.

39. Li M, Huang T, Li MJ, et al. The histone modification reader ZCWPW1 is required for meiosis prophase I in male but not in female mice. *Science advances*. 2019a; 5: eaax1101. doi:10.1126/sciadv.aax1101.

40. Perry J and Zhao Y. The CW domain, a structural module shared amongst vertebrates, vertebrate-infecting parasites and higher plants. *Trends in biochemical sciences*. 2003; 28: 576-80. doi:10.1016/j.tibs.2003.09.007.

41. Liu Y, Tempel W, Zhang Q, et al. Family-wide Characterization of Histone Binding Abilities of Human CW Domain-containing Proteins. *The Journal of biological chemistry*. 2016; 291: 9000-13. doi:10.1074/jbc.M116.718973.

42. He F, Umehara T, Saito K, et al. Structural insight into the zinc finger CW domain as a histone modification reader. *Structure*. 2010; 18: 1127-39. doi:10.1016/j.str.2010.06.012.

43. Hoppmann V, Thorstensen T, Kristiansen PE, et al. The CW domain, a new histone recognition module in chromatin proteins. *The EMBO journal*. 2011; 30: 1939-52. doi:10.1038/emboj.2011.108.

44. Smagulova F, Gregoretti IV, Brick K, Khil P, Camerini-Otero RD and Petukhova GV. Genome-wide analysis reveals novel molecular features of mouse recombination hotspots. *Nature*. 2011; 472: 375-8. doi:10.1038/nature09869.

45. Segurel L. The complex binding of PRDM9. *Genome biology*. 2013; 14: 112. doi:10.1186/gb-2013-14-1-112
10.1186/gb-2013-14-4-112.

46. Billings T, Parvanov ED, Baker CL, Walker M, Paigen K and Petkov PM. DNA binding specificities of the long zinc-finger recombination protein PRDM9. *Genome biology*. 2013; 14: R35. doi:10.1186/gb-2013-14-4-r35.

47. Walker M, Billings T, Baker CL, et al. Affinity-seq detects genome-wide PRDM9 binding sites and reveals the impact of prior chromatin modifications on mammalian recombination hotspot usage. *Epigenetics & chromatin*. 2015; 8: 31. doi:10.1186/s13072-015-0024-6.

48. Khil PP, Smagulova F, Brick KM, Camerini-Otero RD and Petukhova GV. Sensitive mapping of recombination hotspots using sequencing-based detection of ssDNA. *Genome research*. 2012; 22: 957-65. doi:10.1101/gr.130583.111.

49. Stanzione M, Baumann M, Papanikos F, et al. Meiotic DNA break formation requires the unsynapsed chromosome axis-binding protein IHO1 (CCDC36) in mice. *Nature cell biology*. 2016; 18: 1208-20. doi:10.1038/ncb3417.

bioRxiv preprint doi: https://doi.org/10.1101/836023; this version posted November 8, 2019. The copyright holder for this preprint (which was not certified by peer review) is the author/funder, who has granted bioRxiv a license to display the preprint in perpetuity. It is made available under aCC-BY 4.0 International license.

50. Tesse S, Bourbon HM, Debuchy R, et al. Asy2/Mer2: an evolutionarily conserved mediator of meiotic recombination, pairing, and global chromosome compaction. *Genes & development*. 2017; 31: 1880-93. doi:10.1101/gad.304543.117.

51. Kumar R, Oliver C, Brun C, et al. Mouse REC114 is essential for meiotic DNA double-strand break formation and forms a complex with MEI4. *Life science alliance*. 2018; 1: e201800259. doi:10.26508/lsa.201800259.

52. Wahls WP. Meiotic recombination hotspots: shaping the genome and insights into hypervariable minisatellite DNA change. *Current topics in developmental biology*. 1998; 37: 37-75. doi:10.1016/s0070-2153(08)60171-4.

53. Blat Y, Protacio RU, Hunter N and Kleckner N. Physical and functional interactions among basic chromosome organizational features govern early steps of meiotic chiasma formation. *Cell*. 2002; 111: 791-802. doi:10.1016/s0092-8674(02)01167-4.

54. Adams-Cioaba MA and Min J. Structure and function of histone methylation binding proteins. *Biochemistry and cell biology = Biochimie et biologie cellulaire*. 2009; 87: 93-105. doi:10.1139/O08-129.

55. Eidahl JO, Crowe BL, North JA, et al. Structural basis for high-affinity binding of LEDGF PWWP to mononucleosomes. *Nucleic acids research*. 2013; 41: 3924-36. doi:10.1093/nar/gkt074.

56. Rondelet G, Dal Maso T, Willems L and Wouters J. Structural basis for recognition of histone H3K36me3 nucleosome by human de novo DNA methyltransferases 3A and 3B. *Journal of structural biology*. 2016; 194: 357-67. doi:10.1016/j.jsb.2016.03.013.

57. Vezzoli A, Bonadies N, Allen MD, et al. Molecular basis of histone H3K36me3 recognition by the PWWP domain of Brpf1. *Nature structural & molecular biology*. 2010; 17: 617-9. doi:10.1038/nsmb.1797.

58. Mahgoub M, Paiano J, Bruno M, et al. Dual Histone Methyl Reader ZCWPW1 Facilitates Repair of Meiotic Double Strand Breaks. *BioRxiv*. preprint first posted online Oct. 29, 2019. doi:10.1101/821603.

59. Hinch AG, Zhang G, Becker PW, et al. Factors influencing meiotic recombination revealed by whole-genome sequencing of single sperm. *Science*. 2019; 363. doi:10.1126/science.aau8861.

60. Li R, Bitoun E, Altemose N, Davies RW, Davies B and Myers SR. A high-resolution map of non-crossover events reveals impacts of genetic diversity on mammalian meiotic recombination. *Nature communications*. 2019b; 10: 3900. doi:10.1038/s41467-019-11675-y.

61. Wells D, Bitoun E, Moralli D, et al. ZCWPW1 is recruited to recombination hotspots by PRDM9, and is essential for meiotic double strand break repair. *BioRxiv*. preprint first posted online Oct. 30, 2019. doi:10.1101/821678.

62. Peters AH, Plug AW, van Vugt MJ and de Boer P. A drying-down technique for the spreading of mammalian meiocytes from the male and female germline. *Chromosome research : an international journal on the molecular, supramolecular and*

bioRxiv preprint doi: https://doi.org/10.1101/836023; this version posted November 8, 2019. The copyright holder for this preprint (which was not certified by peer review) is the author/funder, who has granted bioRxiv a license to display the preprint in perpetuity. It is made available under aCC-BY 4.0 International license.

evolutionary aspects of chromosome biology. 1997; 5: 66-8. doi:10.1023/a:1018445520117.

63. Bolger AM, Lohse M and Usadel B. Trimmomatic: a flexible trimmer for Illumina sequence data. *Bioinformatics*. 2014; 30: 2114-20. doi:10.1093/bioinformatics/btu170.

64. Langmead B and Salzberg SL. Fast gapped-read alignment with Bowtie 2. *Nature methods*. 2012; 9: 357-9. doi:10.1038/nmeth.1923.

65. DePristo MA, Banks E, Poplin R, et al. A framework for variation discovery and genotyping using next-generation DNA sequencing data. *Nature genetics*. 2011; 43: 491-8. doi:10.1038/ng.806.

66. Li H, Handsaker B, Wysoker A, et al. The Sequence Alignment/Map format and SAMtools. *Bioinformatics*. 2009; 25: 2078-9. doi:10.1093/bioinformatics/btp352.

67. Zhang Y, Liu T, Meyer CA, et al. Model-based analysis of ChIP-Seq (MACS). *Genome biology*. 2008; 9: R137. doi:10.1186/gb-2008-9-9-r137.

68. Robinson JT, Thorvaldsdottir H, Winckler W, et al. Integrative genomics viewer. *Nature biotechnology*. 2011; 29: 24-6. doi:10.1038/nbt.1754.

69. Ramirez F, Ryan DP, Gruning B, et al. deepTools2: a next generation web server for deep-sequencing data analysis. *Nucleic acids research*. 2016; 44: W160-5. doi:10.1093/nar/gkw257.

70. Heinz S, Benner C, Spann N, et al. Simple combinations of lineage-determining transcription factors prime cis-regulatory elements required for macrophage and B cell identities. *Molecular cell*. 2010; 38: 576-89. doi:10.1016/j.molcel.2010.05.004.

71. Zhou Y, Zhou B, Pache L, et al. Metascape provides a biologist-oriented resource for the analysis of systems-level datasets. *Nature communications*. 2019; 10: 1523. doi:10.1038/s41467-019-09234-6.

72. McLean CY, Bristor D, Hiller M, et al. GREAT improves functional interpretation of cis-regulatory regions. *Nature biotechnology*. 2010; 28: 495-501. doi:10.1038/nbt.1630.

bioRxiv preprint doi: https://doi.org/10.1101/836023; this version posted November 8, 2019. The copyright holder for this preprint (which was not certified by peer review) is the author/funder, who has granted bioRxiv a license to display the preprint in perpetuity. It is made available under aCC-BY 4.0 International license.

714 **Figure legends**

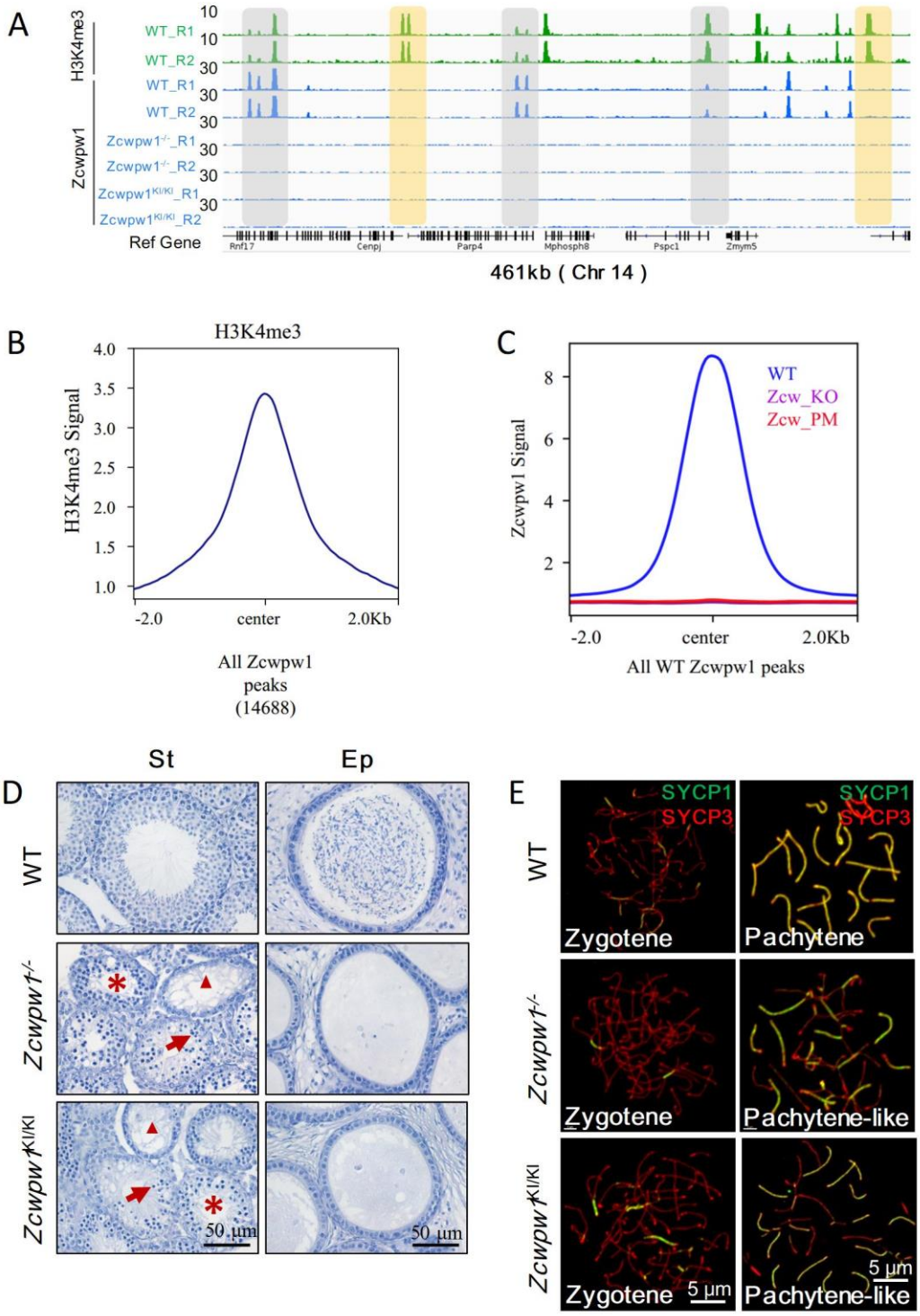

715

716 **Fig.1. ZCWPW1 is an H3K4me3 reader and its binding at chromosomal axes promotes**

717 **completion of synapsis**

bioRxiv preprint doi: https://doi.org/10.1101/836023; this version posted November 8, 2019. The copyright holder for this preprint (which was not certified by peer review) is the author/funder, who has granted bioRxiv a license to display the preprint in perpetuity. It is made available under aCC-BY 4.0 International license.

(A). ChIP-seq genome snapshot of the distribution of H3K4me3 and ZCWPW1 binding peaks in C57BL/6 wild type, *Zcwpw1*$^{-/-}$, and *Zcwpw1*$^{KI/KI}$ mice along a 461-kb-long region of Chromosome 14. H3K4me3 and ZCWPW1 signals were normalized as described in the Methods. Overlapping reads are indicated by grey shaded areas, while non-overlapping reads of interest are indicated by orange shaded areas. **(B)**. Average plot of the H3K4me3 signal in ZCWPW1 ChIP-sequencing peaks; the plot shows the average values over 4-kb intervals for all 14,688 of the detected ZCWPW1 binding regions. **(C)**. Average plot of ZCWPW1 CHIP-sequencing in C57BL/6 wild type and *Zcwpw1*$^{-/-}$ and *Zcwpw1*$^{KI/KI}$ mice. **(D)**. Hematoxylin staining of adult C57BL/6 wild type, *Zcwpw1*$^{-/-}$, and *Zcwpw1*$^{KI/KI}$ testis (right panel) and epididymides (left panel). Adult *Zcwpw1*$^{-/-}$ and *Zcwpw1*$^{KI/KI}$ testis sections showed near complete arrest of spermatogenesis. Arrows, apoptotic spermatocytes; arrowhead, empty seminiferous tubules; asterisk, seminiferous tubules lack of post-meiotic spermatocytes. The spermatogenic arrest led to empty epididymides in adult *Zcwpw1*$^{-/-}$ and *Zcwpw1*$^{KI/KI}$ mice. (St) Seminiferous tubules, (Ep) Epididymides. **(E)**. Chromosome spreads of spermatocytes from the testis of PD60 WT (upper panel), *Zcwpw1*$^{-/-}$ (middle panel), and *Zcwpw1*$^{KI/KI}$ (lower panel) males were immunostained for the SC marker proteins SYCP1 (green) and SYCP3 (red). The arrow indicates a pachytene spermatocyte in WT mice, with complete synapsed chromosomes, arrowheads indicate the pachytene-like spermatocytes in adult *Zcwpw1*$^{-/-}$ and *Zcwpw1*$^{KI/KI}$ mice with incompletely synapsed chromosomes.

bioRxiv preprint doi: https://doi.org/10.1101/836023; this version posted November 8, 2019. The copyright holder for this preprint (which was not certified by peer review) is the author/funder, who has granted bioRxiv a license to display the preprint in perpetuity. It is made available under aCC-BY 4.0 International license.

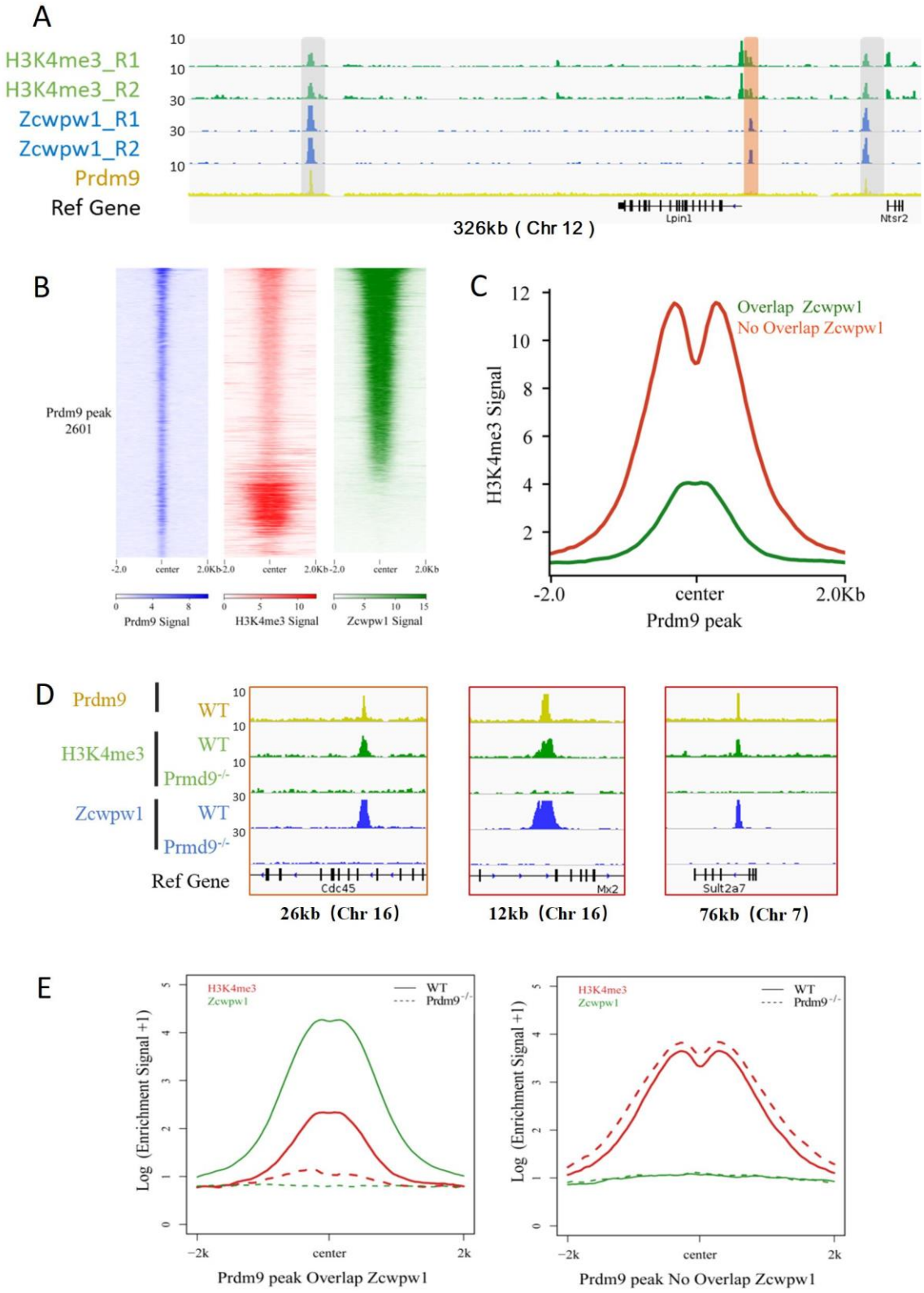

Fig. 2. ZCWPW1 binding is strongly promoted by the histone modification activity of PRDM9

bioRxiv preprint doi: https://doi.org/10.1101/836023; this version posted November 8, 2019. The copyright holder for this preprint (which was not certified by peer review) is the author/funder, who has granted bioRxiv a license to display the preprint in perpetuity. It is made available under aCC-BY 4.0 International license.

(A). ChIP-seq genome snapshot of the distribution of bindings peaks for H3K4me3, ZCWPW1, and PRDM9 in C57BL/6 mice along a 326-kb-long region of Chromosome 12. Overlapping binding peaks in samples from all three analyses are indicated by grey shaded areas, while non-overlapping reads of interest are indicated by orange shaded areas. **(B)**. Heatmap showing the correlation among H3K4me3, ZCWPW1, and PRDM9 binding peaks; each row represents the marker signal among the PRDM9 peaks (2601). **(C).** A profile plot (lower panel) showing the H3K4me3 signal between PRDM9 ChIP-sequencing peaks overlapping with ZCWPW1, or peaks lacking overlap with ZCWPW1. **(D)**. Genome snapshot to show changes in H3K4me3 and ZCWPW1 binding distributions following *Prdm9* knockout. **(E)**. A profile plot showing changes in H3K4me3 and ZCWPW1 binding distributions following *Prdm9* knockout.

bioRxiv preprint doi: https://doi.org/10.1101/836023; this version posted November 8, 2019. The copyright holder for this preprint (which was not certified by peer review) is the author/funder, who has granted bioRxiv a license to display the preprint in perpetuity. It is made available under aCC-BY 4.0 International license.

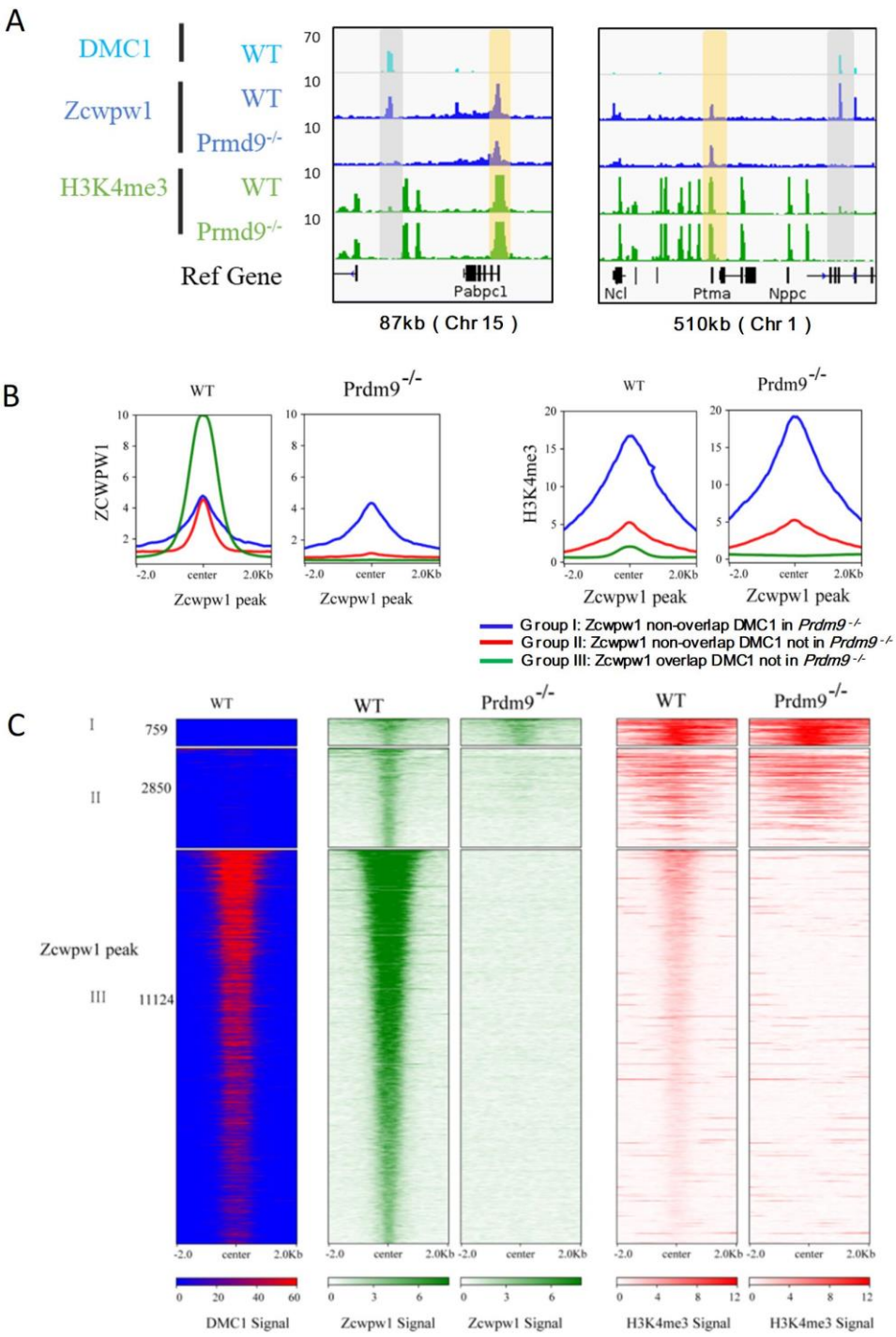

Fig. 3. ZCWPW1 localizes to DMC1-labelled DSB hotspots and does so in a PRDM9-dependent manner

(A). ChIP-seq genome snapshot of the distribution of binding peaks for ZCWPW1, H3K4me3, and DMC1 in C57BL/6 mice, and changes in the ZCWPW1 binding site distributions in *Prdm9* knockout mice. ZCWPW1 and DMC1 overlapping reads are indicated by grey shaded areas, while non-

bioRxiv preprint doi: https://doi.org/10.1101/836023; this version posted November 8, 2019. The copyright holder for this preprint (which was not certified by peer review) is the author/funder, who has granted bioRxiv a license to display the preprint in perpetuity. It is made available under aCC-BY 4.0 International license.

overlapping reads of interest are indicated by orange shaded areas. (**B**). A typical profile showing the overlap of ZCWPW1 and H3K4me3 binding peak overlap with DMC1 or non-overlap with DMC1 changes in *Prdm9* knockout mice. (**C**). Heatmap showing ZCWPW1 and H3K4me3 overlap with DMC1 binding peaks or non-overlap with DMC1 peaks change in *Prdm9* knockout mice. Group I (759) represents ZCWPW1 peaks non-overlapping DMC1 still existing in *Prdm9* knockout mice; group II (2850) represents ZCWPW1 peaks non-overlapping DMC1 lost in *Prdm9* knockout mice; group III (11124) represents ZCWPW1 peaks overlapping DMC1 lost in *Prdm9* knockout mice.

bioRxiv preprint doi: https://doi.org/10.1101/836023; this version posted November 8, 2019. The copyright holder for this preprint (which was not certified by peer review) is the author/funder, who has granted bioRxiv a license to display the preprint in perpetuity. It is made available under aCC-BY 4.0 International license.

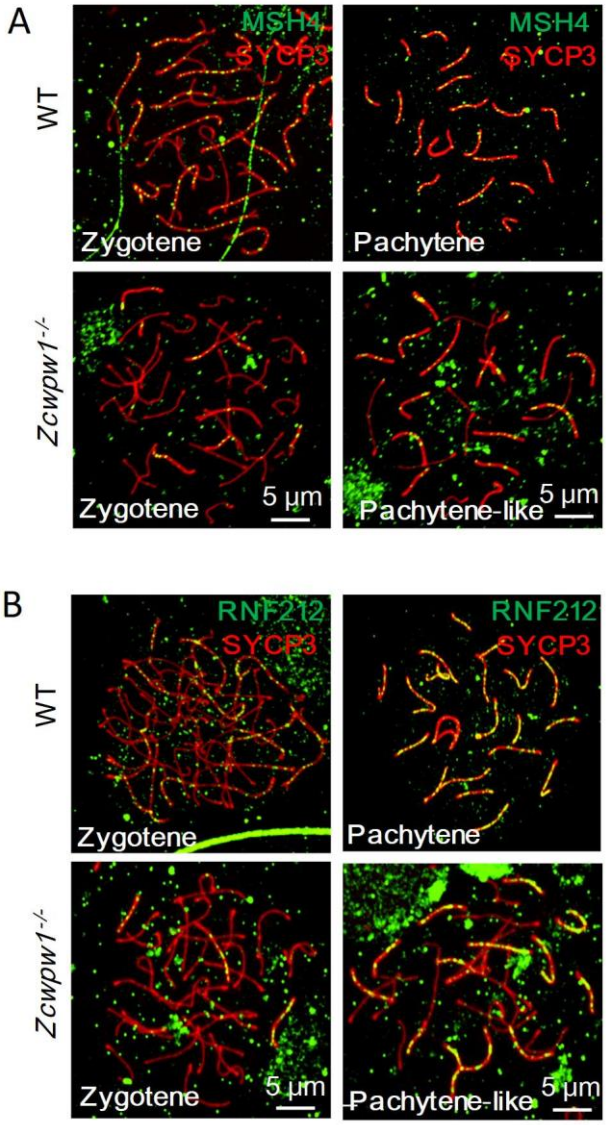

Fig. 4. ZCWPW1 is required for meiotic DSB recombination

(A). Chromosome spreads of spermatocytes from the testis of PD60 WT and *Zcwpw1*$^{-/-}$ males immunostained for the recombination factor MSH4 (green) and the SC marker SYCP3 (red). **(B)**. Chromosome spreads of spermatocytes from WT and *Zcwpw1*$^{-/-}$ males immunostained for the recombination factor RNF212 (green) and the SC marker SYCP3 (red). Representative images are shown for spermatocytes at the zygotene, pachytene, and pachytene-like stages of the two genotypes.

bioRxiv preprint doi: https://doi.org/10.1101/836023; this version posted November 8, 2019. The copyright holder for this preprint (which was not certified by peer review) is the author/funder, who has granted bioRxiv a license to display the preprint in perpetuity. It is made available under aCC-BY 4.0 International license.

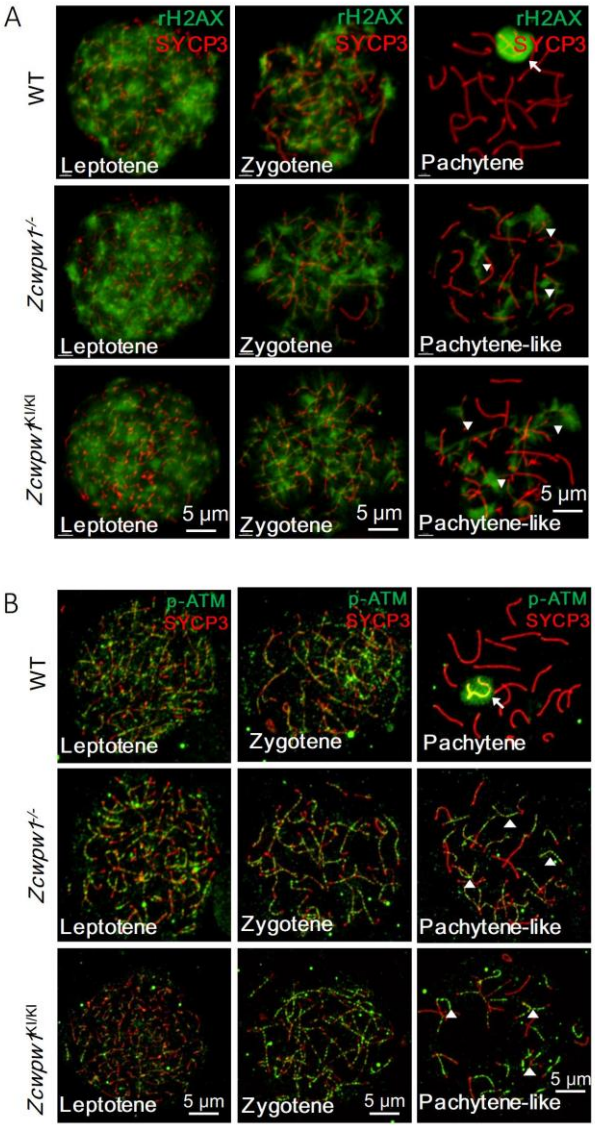

Fig. 5. ZCWPW1 is required for meiotic DSB repair

(A). Chromosome spreads of spermatocytes from the testis of PD60 WT, *Zcwpw1*$^{-/-}$, and *Zcwpw1*$^{KI/KI}$ males immunostained for the DSB marker γH2AX (green) and the SC marker SYCP3 (red). **(B)**. Chromosome spreads of spermatocytes from the testis of PD60 WT, *Zcwpw1*$^{-/-}$, and *Zcwpw1*$^{KI/KI}$ males immunostained for the DSB repair protein p-ATM (green) and the SC marker SYCP3 (red). Representative images are shown for spermatocytes at the leptotene, zygotene, pachytene (arrow indicating the XY body), and pachytene-like (arrowheads indicating the p-ATM signal) stages of the three genotypes.

bioRxiv preprint doi: https://doi.org/10.1101/836023; this version posted November 8, 2019. The copyright holder for this preprint (which was not certified by peer review) is the author/funder, who has granted bioRxiv a license to display the preprint in perpetuity. It is made available under aCC-BY 4.0 International license.

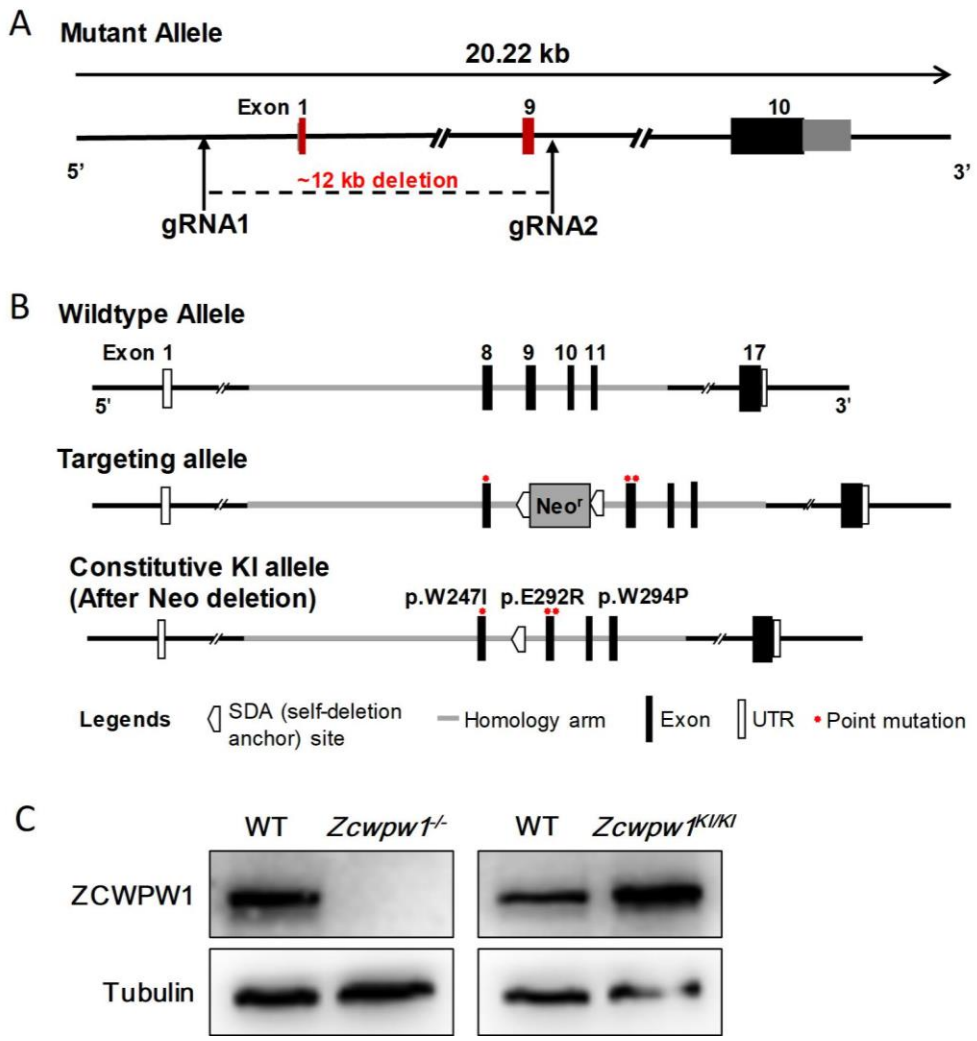

Fig. S1. Generation of Prdm9 knockout mice and Zcwpw1 reader-dead-mutant mice

(A). Schematic representation of the genome CRISP-cas9 editing strategy used to generate the *Prdm9* knockout mice, showing the gRNAs (arrows), the corresponding coding exons (black and red thick lines), and non-coding exons (gray thick lines). Red thick lines (coding exons) represent about 12,000 bp deleted from the wild-type *Prdm9* allele. **(B).** Schematic representation of the genome editing strategy to generate the knock-in *Zcwpw1* reader-dead-mutant mice. **(C).** Western blotting showed that ZCWPW1 was not detected in PD20 *Zcwpw1*$^{-/-}$ testes but was present in wild type testes, and there was a similarly intense signal for *Zcwpw1*$^{KI/KI}$. Tubulin was used as the loading control.

bioRxiv preprint doi: https://doi.org/10.1101/836023; this version posted November 8, 2019. The copyright holder for this preprint (which was not certified by peer review) is the author/funder, who has granted bioRxiv a license to display the preprint in perpetuity. It is made available under aCC-BY 4.0 International license.

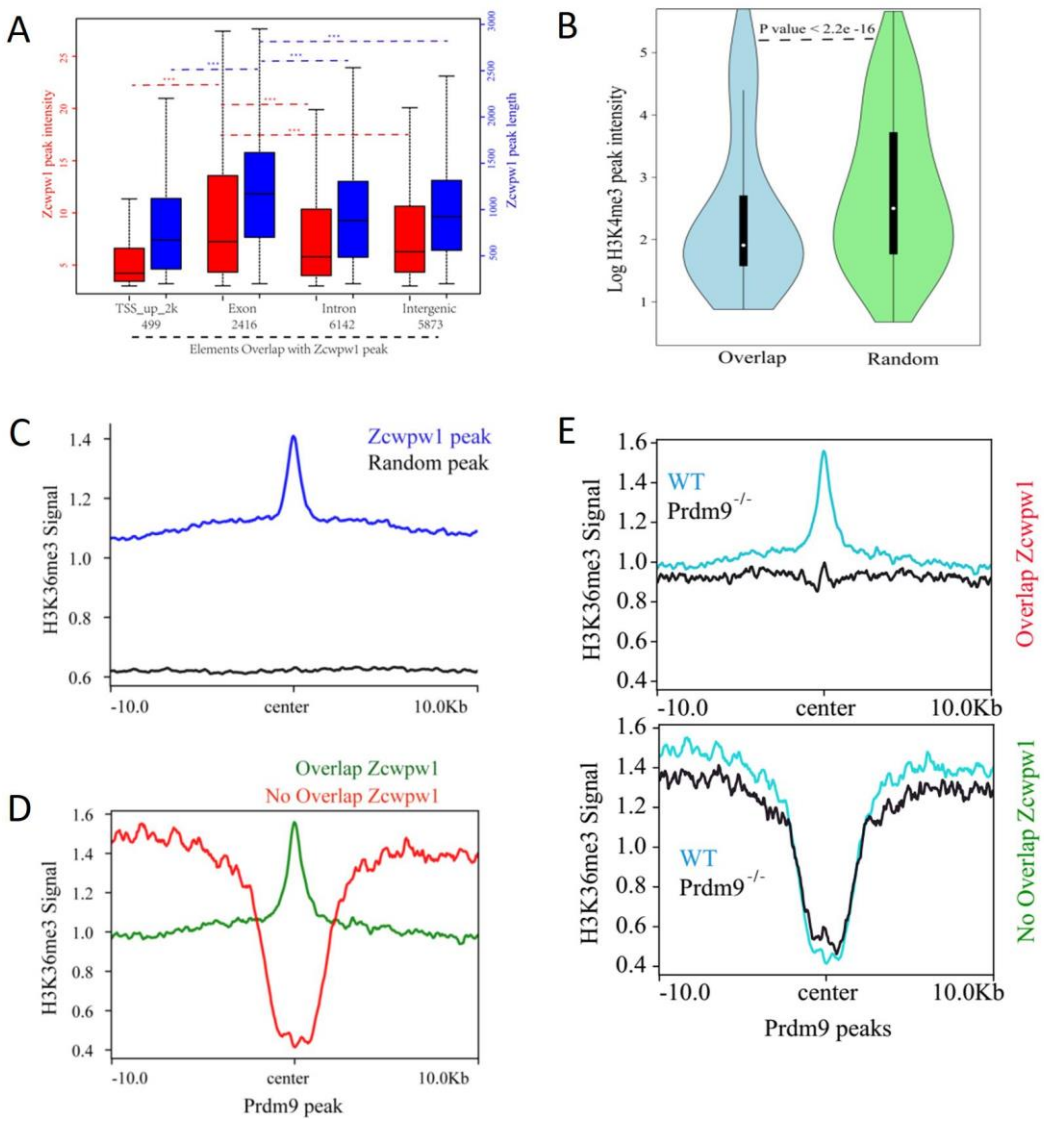

Fig. S2. Correlations between ZCWPW1 peaks and H3K4me3 and H3K36me3 peaks

(A). The distribution of ZCWPW1 peak intensity and peak length for the whole genome. **(B).** A comparison of the H3K4me3 peak intensity between the peaks overlapping ZCWPW1 (5607 peaks) and other, randomly selected H3K4me3 peaks (5607). P value was calculated by Mann-Whitney U test. **(C).** Profile plot to show H3K36me3 signal in ZCWPW1 peaks and random peaks. The plot showed the average values over the 10-kbp interval for all the ZCWPW1 peaks. **(D)**. Profile plot to show H3K36me3 signal in Prdm9 peaks overlapping with Zcwpw1 or without overlapping with ZCWPW1. **(E)**. Profile plot to show H3K36me3 signal in PRDM9 peaks overlapping with ZCWPW1 or without overlapping with ZCWPW1 in wild type and *Prdm9*$^{-/-}$ mice.

bioRxiv preprint doi: https://doi.org/10.1101/836023; this version posted November 8, 2019. The copyright holder for this preprint (which was not certified by peer review) is the author/funder, who has granted bioRxiv a license to display the preprint in perpetuity. It is made available under aCC-BY 4.0 International license.

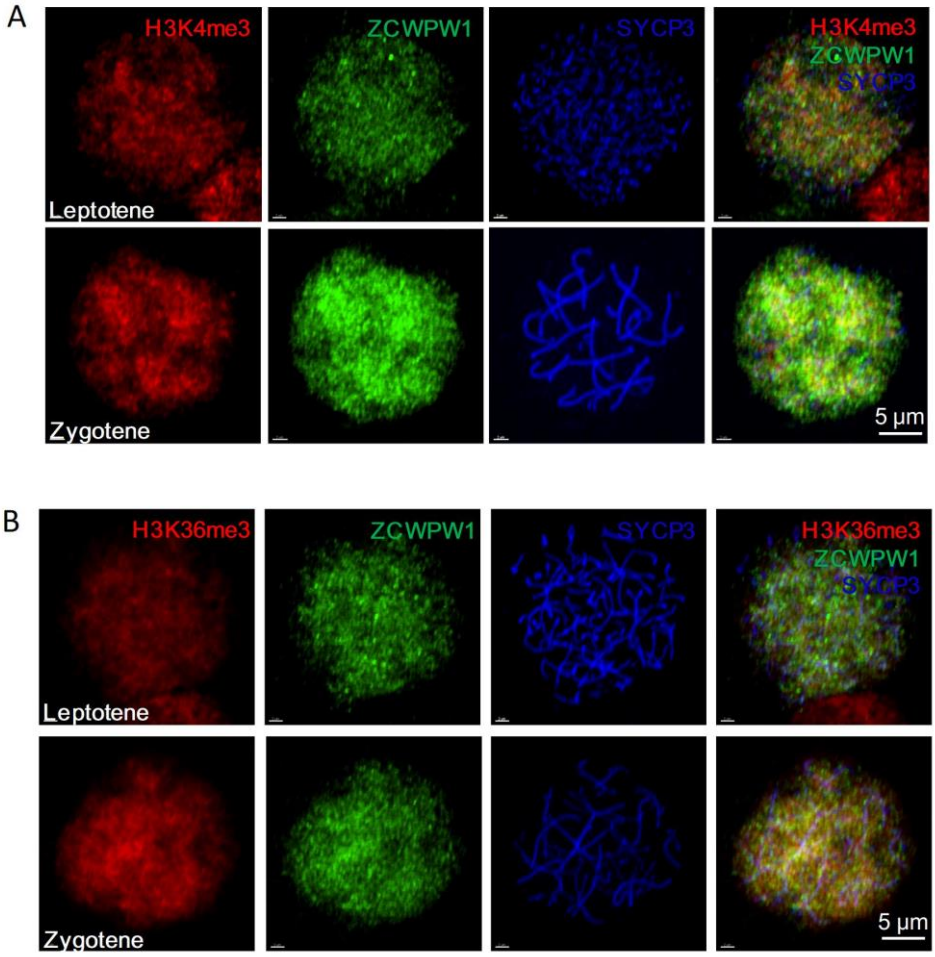

Fig. S3. ZCWPW1 binding peaks correlated with the H3K36me3 peaks at the genome-wide scale **(A)**. Chromosome spreads of spermatocytes from the testes of PD60 wild type were immunostained for H3K4me3 (red), ZCWPW1 (green), and SYCP3 (blue). Representative images of spermatocytes at leptotene and zygotene stages are shown. **(B)**. Chromosome spreads of spermatocytes from the testes of PD60 wild type were immunostained for H3K36me3 (red), ZCWPW1 (green), and SYCP3 (blue). Representative images of spermatocytes at leptotene (upper panels) and zygotene (lower panels) stages are shown.

bioRxiv preprint doi: https://doi.org/10.1101/836023; this version posted November 8, 2019. The copyright holder for this preprint (which was not certified by peer review) is the author/funder, who has granted bioRxiv a license to display the preprint in perpetuity. It is made available under aCC-BY 4.0 International license.

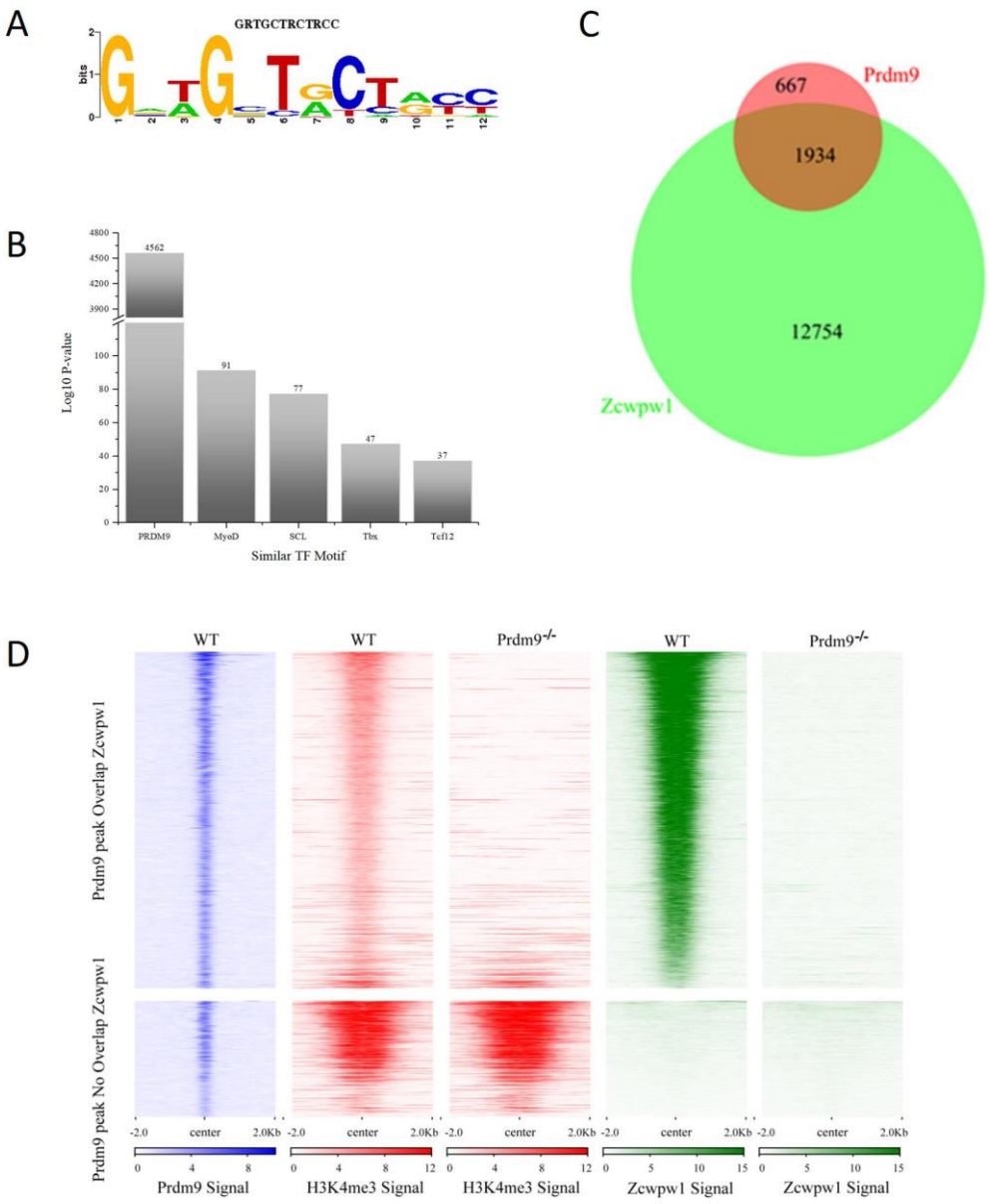

Fig. S4 Correlation between ZCWPW1 chromatin occupancy and PRDM9-induced histone methylation

(A). The *de novo* binding motif of ZCWPW1. **(B)**. The similarity of this ZCWPW1 binding motif with those of other transcription factors. **(C)** Venn diagram (upper panel) showed the overlap of PRDM9 ChIP-sequencing peaks and ZCWPW1 ChIP-sequencing peaks in C57BL/6 mice. **(D)**. The heatmap to show H3K4me3 and ZCWPW1 peaks change following *Prdm9* knockout.

bioRxiv preprint doi: https://doi.org/10.1101/836023; this version posted November 8, 2019. The copyright holder for this preprint (which was not certified by peer review) is the author/funder, who has granted bioRxiv a license to display the preprint in perpetuity. It is made available under aCC-BY 4.0 International license.

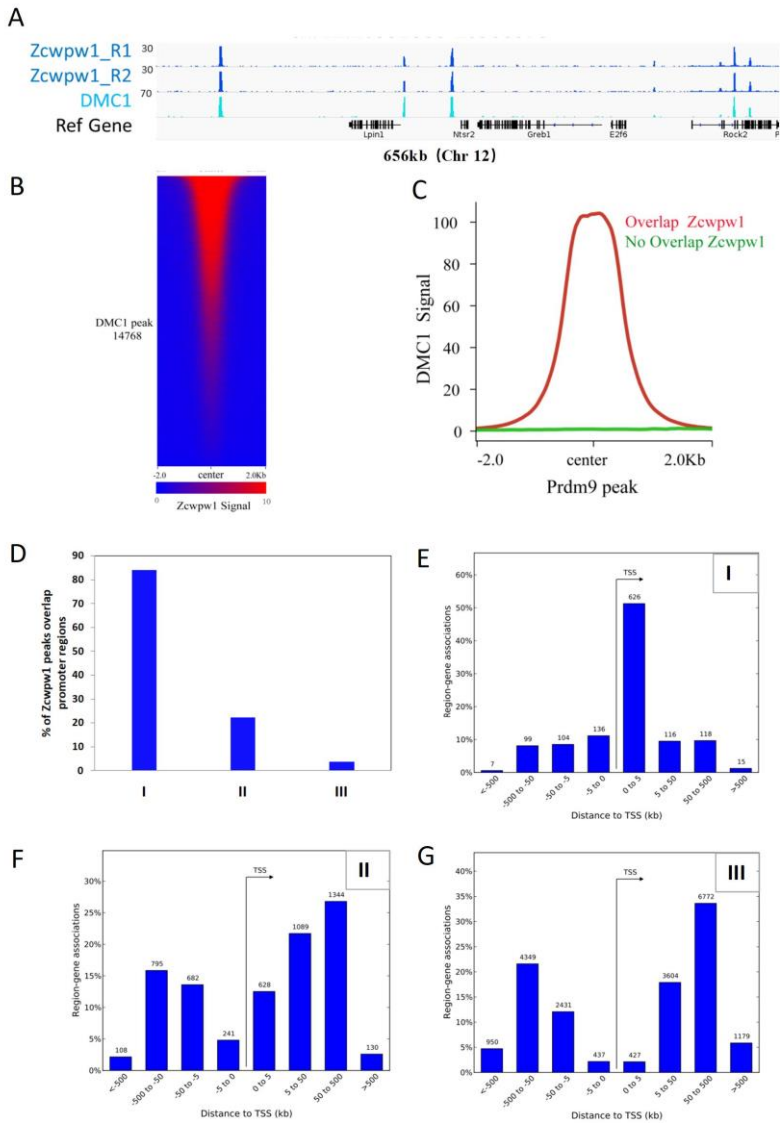

Fig. S5 Correlation between the chromatin occupancy of ZCWPW1 and DMC1

(A). Genome snapshot to show ZCWPW1 and DMC1 peak co-localization in C57BL/6 mice along a 657-kb-long region of Chromosome 12. **(B)**. Heatmap of the ZCWPW1 signal among the DMC1 peaks. **(C)**. The profile plot showed the DMC1 signal in PRDM9 ChIP-sequencing peaks overlapping with ZCWPW1 or without overlapping with ZCWPW1. **(D)**. The percentage of ZCWPW1 peaks overlapping with gene promoter regions in group I, II, III, details in Fig. 3B-C. **(E-G)**. The distance of ZCWPW1 peaks in group I, II, III from protein coding genes within a 1000 kb region.

bioRxiv preprint doi: https://doi.org/10.1101/836023; this version posted November 8, 2019. The copyright holder for this preprint (which was not certified by peer review) is the author/funder, who has granted bioRxiv a license to display the preprint in perpetuity. It is made available under aCC-BY 4.0 International license.

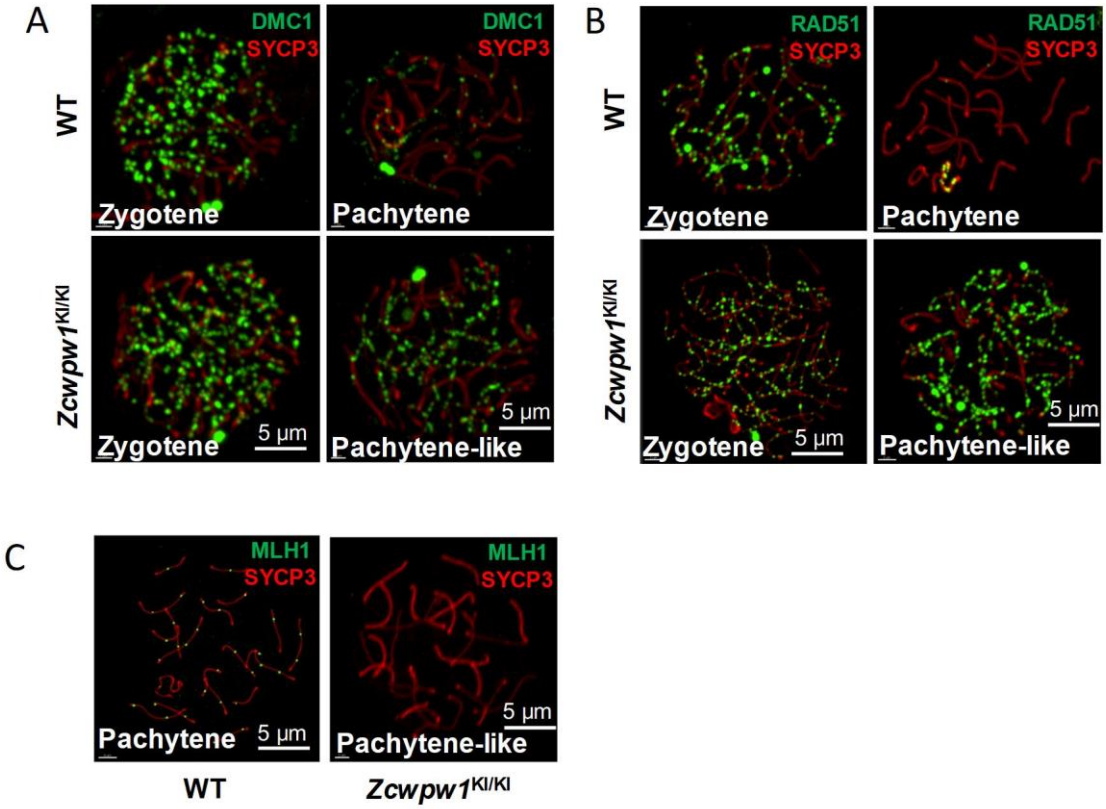

Fig. S6 Meiotic recombination defects in *Zcwpw1* knock-in mice

(A). Chromosome spreads of spermatocytes from the testis of PD70 WT and *Zcwpw1*$^{KI/KI}$ males were immunostained for DMC1 (green) and SYCP3 (red). **(B)**. Chromosome spreads of spermatocytes from the testis of PD70 WT and *Zcwpw1*$^{KI/KI}$ males were immunostained for RAD51 (green) and SYCP3 (red). Representative images of spermatocytes at zygotene, pachytene in WT and zygotene, pachytene-like stages in *Zcwpw1*$^{KI/KI}$ are shown. **(C)**. Chromosome spreads of spermatocytes from the testis of PD60 WT and *Zcwpw1*$^{KI/KI}$ males were immunostained for MLH1 (green) and SYCP3 (red). Representative images of spermatocytes at pachytene in WT and pachytene-like stages in *Zcwpw1*$^{KI/KI}$ are shown.